# Biomimetic photocatalysts for the transformation of CO2: design, properties, and mechanistic insights

Yakubu Adekunle Alli, Nokuthula Magida, Funeka Matebese, Nuria Romero, Adeniyi Sunday Ogunlaja, Karine Philippot

# Biomimetic photocatalysts for the transformation of $CO_2$: Design, properties and mechanistic insights

Yakubu Adekunle Alli[a,b*], Nokuthula E. Magida[c], Funeka Matebese[c], Nuria Romero[a], Adeniyi Sunday Ogunlaja[c], Karine Philippot[a]

[a] CNRS, LCC (Laboratoire de Chimie de Coordination), UPR8241, Université de Toulouse, UPS, INPT, Toulouse cedex 4 F-31077, France.

[b] Department of Chemical Sciences, Faculty of Science and Computing, Ahman Pategi University, Patigi-Kpada Road, Patigi, Kwara State, Nigeria

[c] Department of Chemistry, Nelson Mandela University, Gqeberha (Port Elizabeth), South Africa

[*]Corresponding authors's e-mail address: yakubu.alli@lcc-toulouse.fr;

## Abstract

The increase in $CO_2$ concentration in the atmosphere due to the intensive burning of fossil fuels, for the needs in energy of our modern society, has strongly contributed to the global warming. One of the promising strategies to fight this menace is to capture atmospheric $CO_2$ and convert it into value added products, including fuels and chemicals. Among the methods developed for the transformation of $CO_2$, the sunlight-activated photocatalytic conversion appears as the renewable and easy to use method. For this purpose, it is required to have at disposal proper materials to act as catalysts and light absorbing materials to harvest the sun energy, and then to combine these components with an electron carrier, in an efficient way in order to access the desired fuels by a photocatalytic sustainable $CO_2$ conversion. Among the efforts in research dedicated to the production of solar fuels, studies focused on the design and development of bio-based photocatalytic systems as alternative to conventional photocatalytic systems have emerged in the literature in the last decade. The objective of this review is to show the readers the recent advances in the fabrication of bio-based photocatalysts for the transformation of $CO_2$ into value added products. This review specifically focuses on the conversion of $CO_2$ into carbon monoxide, methanol, formic acid/formate and acetic acid which are the main target products described. Methods adopted to enhance the selectivity and efficiency of the bio-derived photocatalysts developed are also discussed and a section is dedicated to computational

investigations. Finally, the current challenges and perspectives in the development and use of these novel and greener photocatalysts are presented.

**Keyword**s: $CO_2$ transformation; solar fuels; biomimetic photocatalysts; enzymatic catalysis

**Table of contents**



## 1. Introduction

Up to recent period, the burning of fossil fuels has been a major source of energy of our modern society. The inordinate consumption of fossil resources has led to a severe global warming (with new records in the last three years) due to the excessive discharge of greenhouse gasses into the atmosphere, and most particularly of carbon dioxide (O=C=O), and this has become an international crisis that calls for an urgent solution. $CO_2$ is the primary driver of the global warming [1]. In addition, it is a long-lived greenhouse gas, with one-third still present in the atmosphere after a century of release [2]. Scientists believe that if purposeful action is not taken with immediate alacrity to lower $CO_2$ concentration in the atmosphere, global warming and impact of climate change could inevitably lead to the death of more than 250,000 people per year, put 100 million people into abject poverty by 2030 and displace 150 million people or more by 2050 [3]. The transformation of atmospheric $CO_2$ is a herculean task because of its high stability. However, it may have significant benefits in terms of access to carbon based platform molecules and fuels [4]. Among the various strategies available for the reduction of $CO_2$, photocatalytic transformation of $CO_2$ is unarguably a promising and green strategy that could solve the global challenge [5]. The reduction of $CO_2$ by photocatalysis is similar in mechanism to the natural photosynthesis, which can be explained using three separate but linked steps: (i) the

absorption of solar energy (ii) the separation of charges and (iii) surface redox reaction. Utilization of the ubiquitous solar energy in order to reduce $CO_2$ into renewable value-added products would in turn simultaneously improve the lingering global energy shortage, climate change and take a step towards the circular economy [6]. However, the major bottlenecks of existing photocatalysts (i.e. monocatalysts, liquid state Z-scheme, all solid states Z-scheme, direct Z-scheme and type II heterojunctions) are (1) fast recombination of photogenerated charge carriers, (2) poor redox power and (3) Inefficient charge separation thereby hindering the practical application of the technique [7–9]. According to general agreement, a good photocatalytic system must have quick charge transition, efficient charge separation, and good absorption in the visible spectrum, be composed of non-toxic elements and display high stability [10]. Among the photocatalysts reported in the literature, bio-based photocatalysts have gained popularity in the recent decade. This is mainly due to their high reaction efficiency and their fascinating catalytic mechanism inspired by nature [11]. In comparison to their photosynthetic counterparts, non-photosynthetic organisms, especially those created in contemporary synthetic biology, have more desirable metabolic pathways, providing a tunable $CO_2$ metabolism for a variety of products [12]. Other interests of the bio-based photocatalytic systems for the transformation of $CO_2$ into hydrocarbon fuels emerge from the abundance of the biomaterials used, environmental friendliness, and energy-saving if the process is activated by sunlight, to mention but a few. In the reviewing exercises that cover materials for application as catalysts in the transformation of $CO_2$, the recent advancements in the use of bio-based photocatalysts is only little highlighted. For example, Yau and co-workers [13] recently published an updated review which gives precedence to microbial hybrid photosystems for $CO_2$ fixation. Notwithstanding, the review work did not provide elaborate survey on other bio-based photocatalysts and it fails to address the theoretical investigation in order to rationalize the mechanism of $CO_2$ reduction.

In order to sensitize the scientific community to the advantages of using bio-derived photocatalysts (i.e. a natural light driven catalytic reaction using enzyme, bacterial and polymers) for the conversion of $CO_2$, this review intends to gather the recent research (i.e. covering the last decade) on the design of such photocatalytic systems for the transformation of $CO_2$ into fuels. The examples reported are classified into five sections in line with the target hydrocarbon fuel, namely carbon monoxide, methanol, formic acid/formate and acetic acid (see sections 2, 3, 4 and 5, respectively). Furthermore, in section 6, an in-depth analysis on the interest of computational

investigations for the development of bio-derived photocatalysts for $CO_2$ reduction is given. Computational data may either complement or to give prior understanding into experimental investigations. Finally, current challenges and future outlook are discussed.

## 2. Biomimetic photocatalysts for the transformation of $CO_2$ to carbon monoxide

Carbon monoxide (CO) is one of the attractive value-added products that can be generated from the reduction of $CO_2$. It is commonly used as an intermediate in some chemical processes including the production of drugs, fragrances, formaldehyde or benzaldehyde and methanol [14]. Some chemical industries also use CO in the preparation of inorganic chemicals such as metal carbonyls like nickel tetracarbonyl (**Eq. 1**) and iron pentacarbonyl (**Eq. 2**).

$$Ni + 4CO \rightarrow Ni(CO)_4 \quad (1)$$

$$Fe + 5CO \rightarrow Fe(CO)_5 \quad (2)$$

Furthermore, CO plays an important role alongside with hydrogen gas, forming together the syngas that is used in the Fischer-Tropsch process towards superior hydrocarbons [15].

From thermodynamic and kinetic points of view, the generation of CO from $CO_2$ is one of the easiest compared to that of other hydrocarbon fuels. The reduction of $CO_2$ into CO and $H_2O$ requires two electrons and two protons with a reduction potential of 0.53V (vs. NHE at pH = 7) (**Eq. 3**).

$$CO_2 + 2H^+ + 2e^- \rightarrow CO + H_2O \quad E = 0.53V \quad (3)$$

Different bio-based photocatalytic materials have been employed for the conversion of $CO_2$ to CO. In one of the earliest studies, Woolerton et al. developed a photocatalytic system that comprises metal-oxide nanoparticles functionalized by the enzyme carbon monoxide dehydrogenase (CODH) as catalyst and sensitized to visible light by a ruthenium bipyridyl photosensitizer, both components being supported on an anatase/rutile $TiO_2$ mixture as the semiconductor (electron donor). Using this photocatalyst activated by visible light they could effectively reduce $CO_2$ to CO [16]. The authors examined the CO production rates and stability as a function of each component (photosensitizer, enzyme and $TiO_2$). Tolerance to $O_2$ and effects of different electron donors were also investigated, together with strategies to control enzyme binding at the surface of $TiO_2$ in order to enhance overall activity (**Fig. 1a**). Ding and co-authors [17] reported a functional porous coordination hybrid system composed of nickel porphyrin and

nickel bis(terpyridine) dual active sites as efficient bio-based photocatalyst for $CO_2$ reduction into CO under the illumination of visible light ($\lambda \geq 420$ nm) (**Fig. 1b)**. The biomaterials exhibited an extraordinary photocatalytic activity towards the CO formation with an outstanding generation rate of 3900 $\mu molh^{-1}g^{-1}$ and selectivity of 98%. Also, they investigated the mechanism of action associated with dual active sites of the system, composed of metal porphyrin and metal bis(terpyridine), using theoretical simulations which further supported an excellent photocatalytic performance of these bio-hybrids as observed in the experimental investigation (**Fig. 1c**). The theoretical investigation demonstrated that the binding between $CO_2$ and Ni(II) in nickel bis(terpyridine) is much easier than that with nickel porphyrin. The Ni−C Mayer bond order of $*CO_2$ intermediate in nickel bis(terpyridine) was 0.533, much higher than that (0.009) in nickel porphyrin, which accounts for the stability of the intermediate of the former.

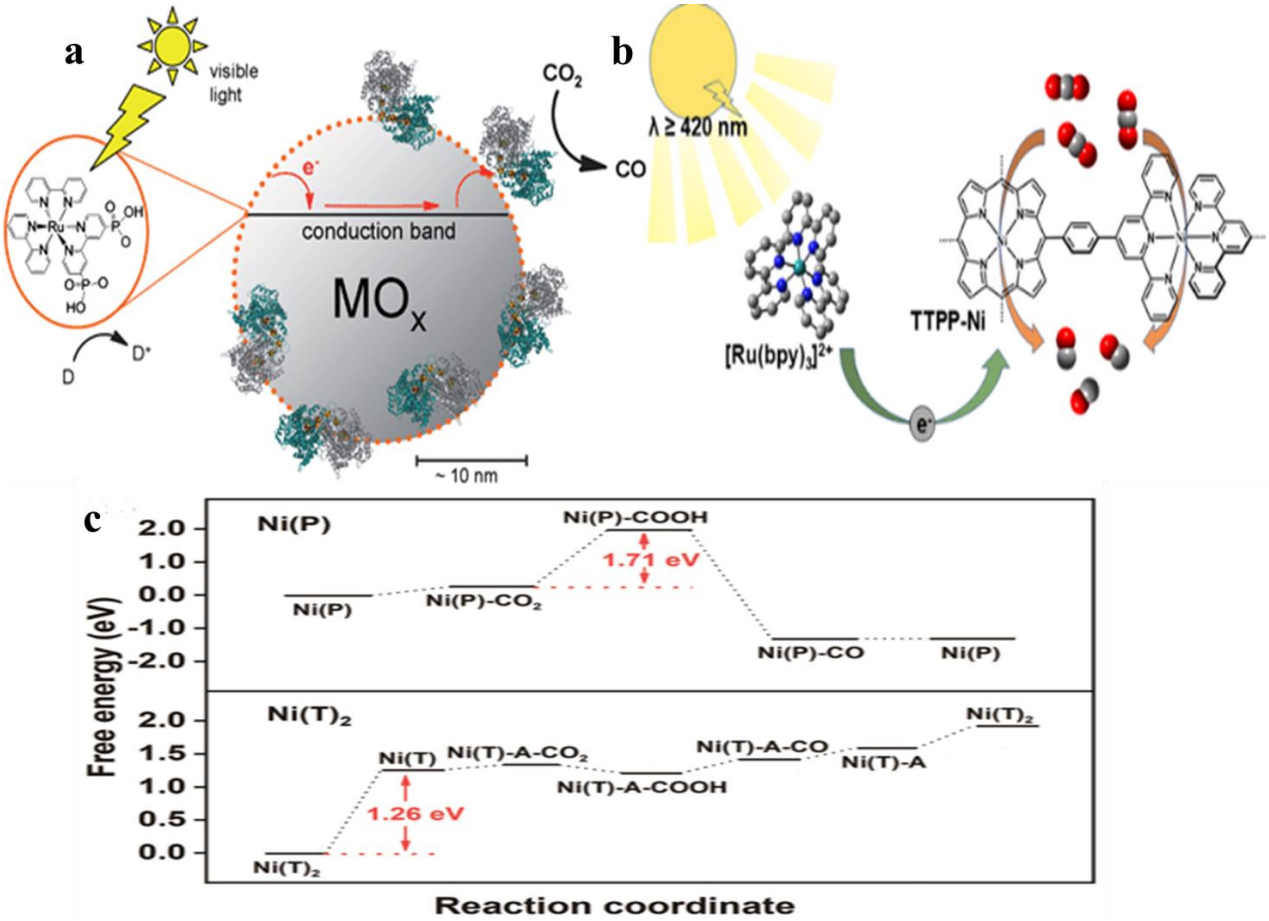

**Figure 1.** Mechanism of $CO_2$ reduction to CO by (a) CODH/ruthenium bipyridyl/anatase or rutile-$TiO_2$. Reproduced with the permision from [16]. Copyright 2011 Royal Society of Chemistry. (b) Ni Porphyrin and Ni bis(terpyridine) coordinated polymer (TPP-Ni) (c) Schematic mechanism of $CO_2$ reduction catalyzed by Ni Porphyrin and Ni bis(terpyridine) . Adapted with the permission from [17]. Copyright 2022 American Chemical Society.

In a related study, Liang and co-workers [11] developed a biomimetic system based on metalloporphyrin and $ZrO_2$ nanoframes that showed an evolution CO yield of 35.3 µmol within 3 h of reaction and high selectivity rate of 93.1% as well as an apparent quantum efficiency of 1.84% which is 60.8 greater than pristine porphyrin-Ni with evolution rate of 0.58 µmol.

The group of Zhao [18] constructed a covalently bonded reaction centre bio-hybrids comprised of Co-based porphyrin and a low molecular mass graphitic $C_3N_4$ for the transformation of $CO_2$ to CO under the irradiation of visible light. They obtained a photocatalytic activity 13 times greater than that of pure $C_3N_4$ (CO generation rate of 17 $\mu molg^{-1}h^{-1}$), thus evidencing the positive role of the Co porphyrin. The improved activity was attributed to the efficient electron transfer and trapping by CO active sites, improved electron-hole separation and strong affinity of Co-porphyrin for $CO_2$ adsorption.

Lin and colleagues [19] designed a highly efficacious g-$C_3N_4$/tetra(4-carboxyphenyl)porphyrin (III) chloride heterogeneous catalyst for selective photoreduction of $CO_2$ into CO under visible light (**Fig. 2a**). In this catalytic system they used abundant, environmentally friendly FeTCPP as the catalytic center and inexpensive g-$C_3N_4$ nanosheets as the light absorber, maintaining a simple mechanical mix under constant stirring. A maximum rate of 6.52 mmol $g^{-1}$ of CO in 6 h, with up to 98% selectivity was obtained. The catalytic performance was attributed to an effective electron transfer from g-$C_3N_4$ nanosheets to FeTCPP

Apart from the enzymitic/bacterial based photosystems reviewed so far, Zhou and co-authors [20] reported biomimetic polymeric semiconductor based hybrid nanosystems that combined a typical $CO_2$/proton reduction catalyst, a cocatalyst, an electron mediator, and a $CO_2$ activator for artificial photosynthesis with water and $CO_2$. g-$C_3N_4$ nanosheets, which mimic the nanolayered thylakoids stacks, are shown to be promising photocatalytic elements with a planar configuration and a high surface area, and they serve as an excellent platform for the assembly of other

analogous elements (**Fig. 2b**). Au NPs are used as a suitable cocatalyst. ZIF-9 is used as a $CO_2$ concentrator and an electron mediator to promote the redox reaction. The highest production of CO and $H_2$ was achieved by ZIF-9(1%)Au-CNS at the evolution rates of 0.3 and 7.5 $\mu molh^{-1}g^{-1}$, respectively. The study revealed that the incorporation of polymeric based g-$C_3N_4$ and ZIF-9 significantly enhanced the CO evolution rates which is 122 folds higher compared to non-ZIF-9 modified systems.

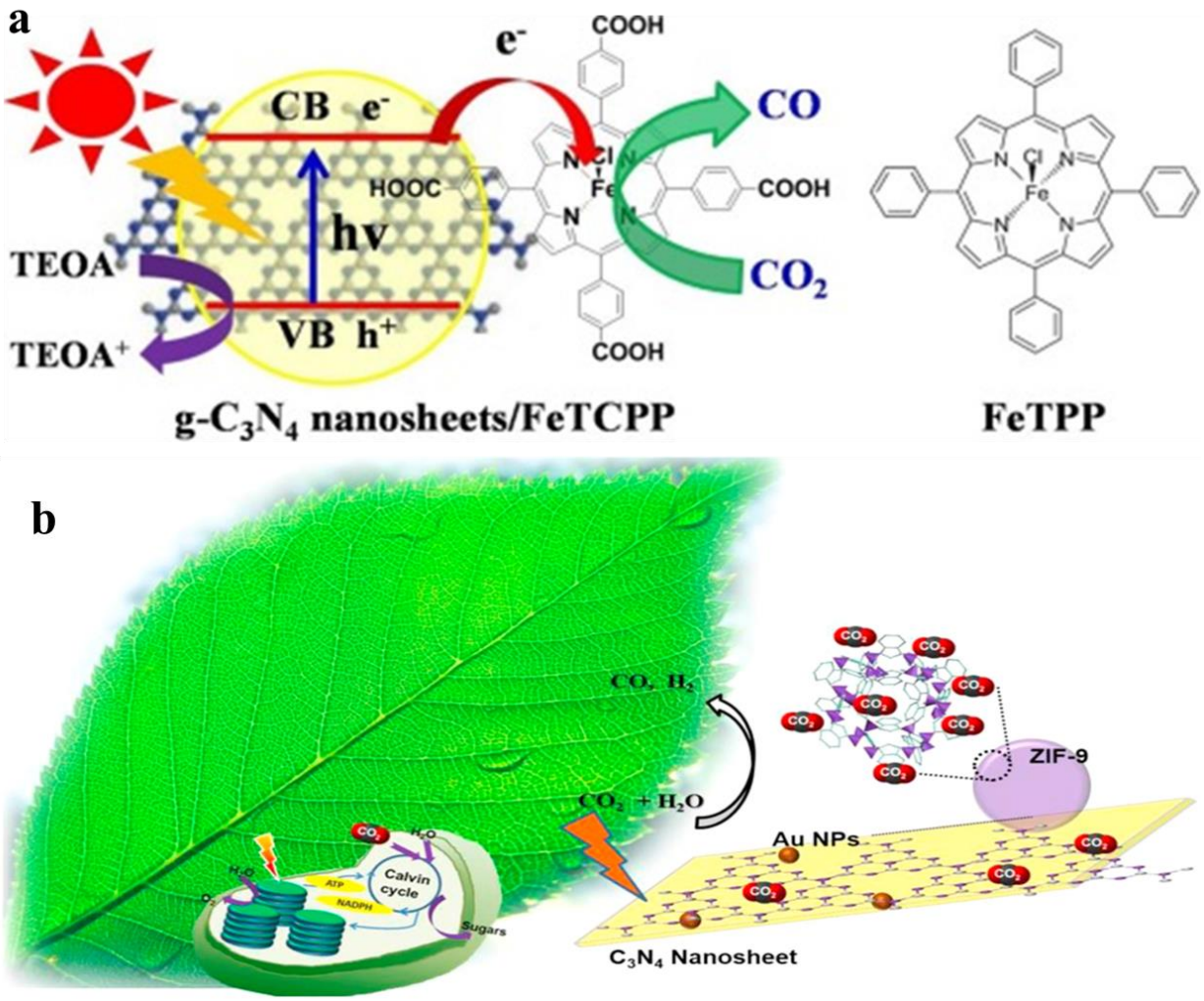


**Figure 2**. Plausible mechanism of $CO_2$ photoreduction by (a) g-$C_3N_4$/FeTCPP hybrids (b) Photoconversion activity of $C_3N_4$/AuNPs/ZIF-9. Reproduced with the permision from [19] and [20] . Copyright 2018, 2016 Elsevier, respectively.

**Table 1** below outlines biomimetic photocatalysts that have been explored for CO production from $CO_2$ reduction. The synergistic incorporation of biomimetic photocatalysts has shown to be promising for the reduction of $CO_2$ to CO with high selectvity. However, the present bio based photocatalytic systems for CO production have not provided satisfactory activity and stability, key points that necessitate further research.

**Table 1**. Carbon monoxide production using bio-based photocatalysts

| **Photocatalytic system** | **Reaction conditions** | **CO yield/TON** | **Comments** | **Reference** |
|---|---|---|---|---|
| TTPP-Ni/metal based bis(terpyridine) with dual active sites | Photocatalytic activity under $\lambda \geq 420$ nm, trisopropanolamine employed as sacrificial agent, 15mg catslyst | 3900 **$\mu molh^{-1}g^{-1}$** | The composites exhibited high CO yield. However, there is partial dissolution of photocatalysts | [17] |
| Zn-porphyrin sensitised Mn (I) | Aqeuous medium, red light irradiation ($\lambda$ = 620 nm) | Low yield | The slow conversion rate of $CO_2$ to CO was atributed to inadequate e- migration from porphyrin to the catalyst | [21] |
| Carbon monoxide dehydrogenase functionalized with CdS nanocrystals | Carried out under viisible light irradiation | Good yield | The size and morphologgy of the nanocrystals greatly | [22] |

| | | | | |
|---|---|---|---|---|
| | | | enhanced the actvity | |
| Nafion assisted Re(I)-RuL | The catalytic activity was done under visibile light for 20h, | 454 **$\mu molh^{-1}g^{-1}$** | The presence of nafion improved the photocatalytic activity | [23] |
| Polymeric based g-$C_3N_4$/AuNPs/ZIF-9 | 80 kPa of pure $CO_2$ gas was purged, 300W Xe arc lamp as light source | 0.4 $\mu molh^{-1}g^{-1}$ | The dominant evoluted gas is $H_2$ which is not favourble for the reaction | [20] |
| g-$C_3N_4$/FeTCPP | Under visible light greater than 420 nm. TEOA was used as sacrificial agent | 6.52 $mmolg^{-1}$ | The findings indicates that the electrons migrated from g-$C_3N_4$ to FeTCPP | [19] |
| $ZrO_2$ nanoframes/metalloporphyrins | Visible light | 35.3 µmol | The bio based material efficiently transfer electrons to the Ni catalytic sites which in turn increased the CO generation | [11] |

TON: Turn over frequency, FeTCPP: tetra(4-carboxyphenyl)porphyrin (III) chloride

## 3. Biomimetic photocatalysts for the transformation of $CO_2$ to methanol

Methanol or methyl alcohol ($CH_3OH$) is an organic compound primarily used as a solvent, co-solvent, or feedstock in the chemical industry. Methanol has an octane number of 113 and a density that is half that of the gasoline, as thus, can be mixed with gasoline with no technical modifications and be used in methanol-fuelled vehicles [24]. Although methanol is considered an environmentally friendly fuel (no oxides of sulphur or nitrogen), the production of CO during its combustion limits its use as a pure fuel (100%). Hence it is mixed with gasoline on a ratio of 85% (methanol) - 15% (unleaded gasoline) [25]. More usages of methanol include hydrogen storage and transportation as an energy carrier as well as an easily transportable fuel, and also production of intermediates and synthetic hydrocarbons as a C1 building block [26]. Methanol is therefore regarded as a transition molecule from fossil fuels to renewable energies.

Methanol can be synthesized from carbon-containing materials such as natural gas, coal, biomass, and carbon dioxide ($CO_2$). Natural gas is currently the primary source of methanol contributing approximately 90% to the world 111 million metric ton production [27]. Unfortunately, natural gas and coal are fossil fuel resources, thus depleting non-renewable resources and significantly contributing to greenhouse gas emissions. The burning of fossil fuels (natural gas, coal, and oil) leads to $CO_2$ emissions which contribute significantly to global warming. Therefore, green production of methanol has gained a great attention of academic and industrial researchers.

Catalytic hydrogenation of $CO_2$ has been proposed as a green methanol production process. This process falls under the carbon capture and utilization (CCU) strategy which uses catalysts in the reaction of $CO_2$ and hydrogen (**Eq. 4**). The transformation of $CO_2$ to methanol is considered a green process when using captured $CO_2$ and/or hydrogen from renewable energy resources. The study by González-Garay et al. [28] shows how much $CO_2$ emissions can be avoided when using the green methanol synthesis process. However, the green methanol production *via* $CO_2$ hydrogenation is not economically feasible compared to the fossil-based process due to high costs of renewable hydrogen [28]. Therefore, there is an urgent need for developing cost effective $CO_2$ conversion technologies to produce methanol in a green way. Amongst many $CO_2$ conversion technologies such as biological, thermochemical, and electrochemical routes, the photochemical process has gained extensive attention [29]. If using solar light as its source of

energy, the photocatalytic reduction of $CO_2$ into valuable chemicals like methanol may be a sustainable approach [30–34].

$$CO_2 + 6H^+ + 6e^- \longrightarrow CH_3OH + H_2O \quad (4)$$

Enzymatic conversion of $CO_2$ requires energy source like for the photochemical processes. The energy sources can be diverse, including ultraviolet, electrical potential, or energy carrying molecules (adenosine triphosphate (ATP), guanosine triphosphate (GTP), nicotinamide adenine dinucleotide (NADH)). While in a photochemical process, an electron donor, a photosensitizer, and catalysts (e.g. $TiO_2$, ZnO, graphene, etc.) are mainly required to drive selective production to methanol [35,36] [37–40]. These photocatalysts may be incorporated into biomaterials such as biochars and biopolymers with conductive properties (e.g. cellulose, chitosan, etc.) to improve their structural and electronic properties [32,41–43]. There have been few case studies on biomimetic photocatalysts for the reduction of $CO_2$ to methanol since 2015 due to cost of enzyme production, regeneration, nonetheless, the research area is slightly increasing (as seen in **Table 2**).

Recently, Tseng and co-workers [44] utilised sugarcane bagasse (SB) to support graphitic carbon nitride (gCN) for photocatalytic reduction of $CO_2$ to CO and methanol using a 14-watt LED light bulb. The presence of lignin in SB resulted in the semiconductor-like absorption edge and provided the interaction with gCN. The use of SB alone for photocatalytic study resulted in the formation of small amounts of MeOH. This is linked to the electronic transition of conjugated species within lignin (from SB) thus providing photoinduced charge carriers on SB. The introduction of SB (containing lignin) influenced the semiconductor-like absorption edge properties of the photocatalyst. Catalyst synthesis, g-SB-HT, using water (g-SB-HT-W) and ethanol (g-SB-HT-E) influenced MeOH yields, as the later solvent may be seen to have acted as hole scavenger thus increasing the yield of methanol (see Table 2).

Tseng and co-workers [45] also developed titanium oxide-chitosan film hybrid material ($TiO_2$-chitosan) for the photocatalytic $CO_2$ reduction to methanol. This $TiO_2$-chitosan material was able to selectively convert $CO_2$ in methanol at a production rate of 0.37 nmol/g (**Table 2**), showing a good stability. Similarly, Kavil and co-workers [46] synthesized a $TiO_2$-based hybrid photocatalyst (Cu-C(glucose)/$TiO_2$) by co-doping $TiO_2$ with copper (from copper sulfate) and carbon (from glucose) to photocatalytically reduce $CO_2$ to methanol. The photocatalytic experiment was performed in a Pyrex glass photoreactor filled with the catalyst and a NaOH

suspension and then purged with certified super–critical fluid grade carbon dioxide for 30 min. The photoreactor was irradiated with UV lamps (365 nm wavelength) for 5 h. In these conditions the Cu-C/$TiO_2$ catalyst allowed to achieve the highest methanol production (~2600 μM) with compared to counterparts C/$TiO_2$ ($TiO_2$ doped with only carbon) and $TiO_2$ P25, thus evidencing the synergy effect between the three components, Cu, C and $TiO_2$.

Studies have shown that enzymes catalysed photoreduction of $CO_2$ to methanol involves using a three-step enzyme cascade including formate dehydrogenase (FDH), formaldehyde dehydrogenase (AldDH or FDH), and alcohol dehydrogenase (ADH) [46]. Co-enzymes and co-factors are usually sacrificial for photoredox reactions and are depleted in the process, thus, requiring enzymes that may regenerate the reduced forms. To further improve methanol yield, sequential and co-immobilization of dehydrogenases with polymeric membranes, metal complexes and oxides have been proposed [47].

Biocatalysts such as enzymes, namely formate (FDH), aldehyde (AldDH), formaldehyde (FalDH), lactate (LDH) and alcohol (ADH) dehydrogenases was tested for $CO_2$ reduction to methanol [47,48]. Co-enzymes (also known as co-factors) such as nicotinamide adenine dinucleotide ($NAD^+$) or its reduced form (NADH) and methylviologen ($MV^{2+}$) are often used with FDH, NADH, AldDH and ADH. [48][49–51]. Amao and co-workers [36] developed a photochemical enzyme-based conversion system for the $CO_2$ photoreduction to methanol, using FDH, AldDH, and ADH combined with $MV^{2+}$ under the visible-light photosensitization of water-soluble porphyrin, tetraphenylporphyrin tetrasulfonate ($H_2TPPS$) in the presence of triethanolamione (TEOA) (**Fig. 3**). This complex photoredox system allowed to achieve a methanol production concentration of 6.8 μM. Study of the enzymatic kinetics evidenced that the rate-limiting step is the formic acid to formaldehyde reaction with AldDH and reduced form of $MV^{2+}$ (Methyl viologen).

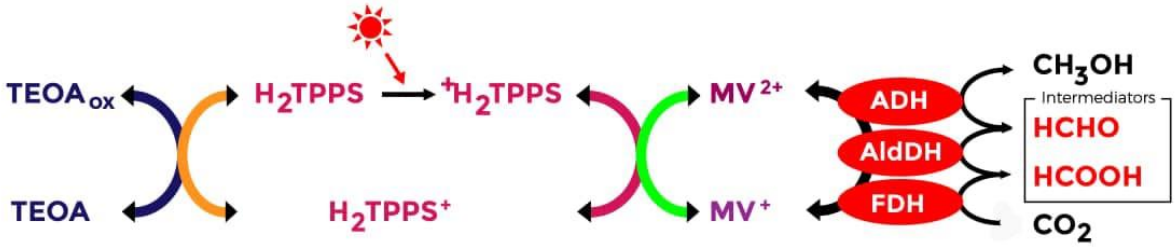


**Figure 3.** Methanol production from $CO_2$ catalysed with $H_2TPPS/MV^{2+}$/TEOA/FDH, AldDH and ADH photoredox system. Reproduced with permission from reference [36]. Copyright 2018 Elsevier.

The use of co-enzyme nicotinamide adenine dinucleotide reduced form (NADH), FDH catalyses both the reduction of $CO_2$ to formic acid, ADH catalyses the reduction of formic acid to formaldehyde, and ADH catalyses both the reduction of formaldehyde to methanol (Fig 4). The resulting co-enzyme nicotinamide adenine dinucleotide ($NAD^+$) catalyses the oxidation of formic acid to $CO_2$, formaldehyde to formic acid and oxidation of methanol to formaldehyde, respectively, thus inhibiting methanol production due to the redox nature of $NAD^+$/NADH (Fig. 4). The oxidation processes were suppressed using oxidized form of $MV^{2+}$, an electron carrier molecule, to drive the photochemical production of methanol. A reaction scheme for methanol production from $CO_2$ with FDH, AldDH and ADH using natural co-enzyme $NAD^+$/NADH and artificial co-enzyme $MV^{2+}/MV^+$ is presented in **Figure 4**.

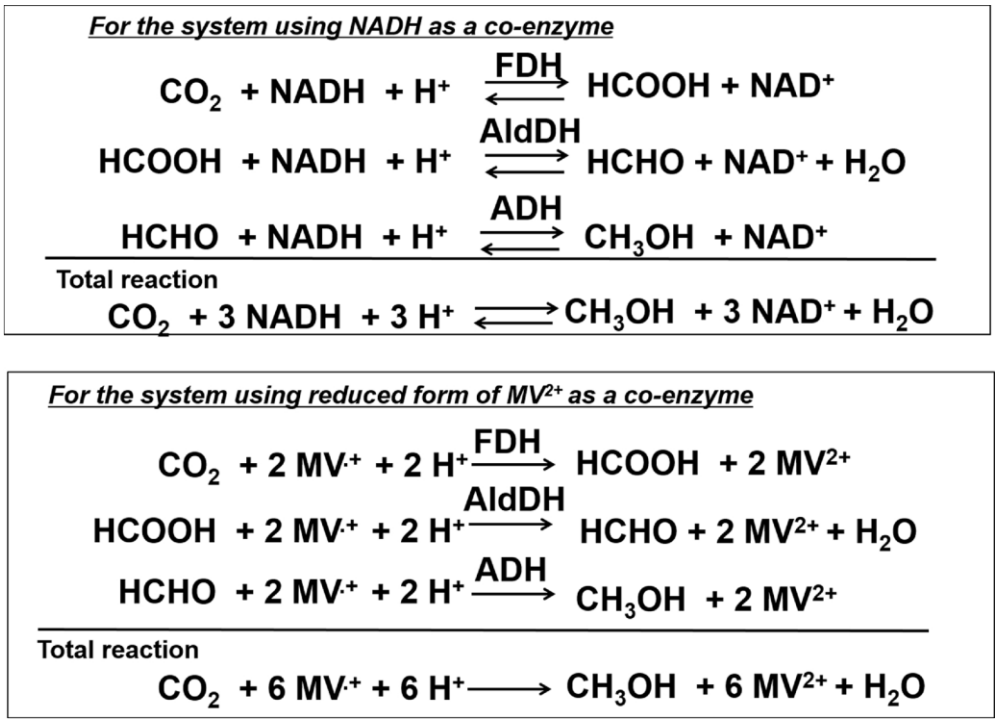


**Figure 4**. Scheme for the methanol production from $CO_2$ with FDH, AldDH and ADH using natural co-enzyme NAD+/NADH and artificial co-enzyme $MV^{2+}/MV^{+}$.

Zezzi Do Valle Gomes and co-workers [48] reported the biocatalytic cascade conversion of $CO_2$ to methanol using three dehydrogenases (FDH, ADH and FalDH) co-immobilized in tailored siliceous mesostructured cellular foams (MCF) functionalized with mercaptopropyl groups (MP) with no cofactor. With this catalytic system they obtained a methanol yield of 0.35 $mmol/g_{enzyme}/min$, a value which might be improven by adding NADH regeneration.

Yadav et al. [52] prepared a CCG-IP type photocatalyst by attaching isatin-porphyrin (IP) chromophores with chemically converted graphene (CCG). A methanol production concentration of 11.21 µM was achieved using CCG-IP under visible light with an NADH photoregeneration of 39%.

Ji et al. [53] developed a polyelectrolyte-doped hollow nanofibers/microcapsules-based integrated photosynthesis system. Basically, the system was designed by assembling the components involved in the electron-transfer chain in a specific order, such that the photo-excited electrons can be transported efficiently in the opposite direction. This system was integrated in a device in the following order: three dehydrogenases and a cofactor (FDH, FalDH,

ADH and NAD(H)) in the innermost layer, electron mediators (M) in the middle layer, a photosensitizer ($EY^-$ Eosin Y) in the outermost layer and an electron donor (TEOA) for the $CO_2$ conversion to methanol under solar energy (depicted in **Fig. 5).** They achieved a methanol production of 60.37 µM (hollow mixture of poly(allylamine hydrochloride) (PAH) and polyurethane (PU) nanofiber-based system) and 61.98 µM (microcapsules-based system) with 86.04% NADH photo-regeneration.

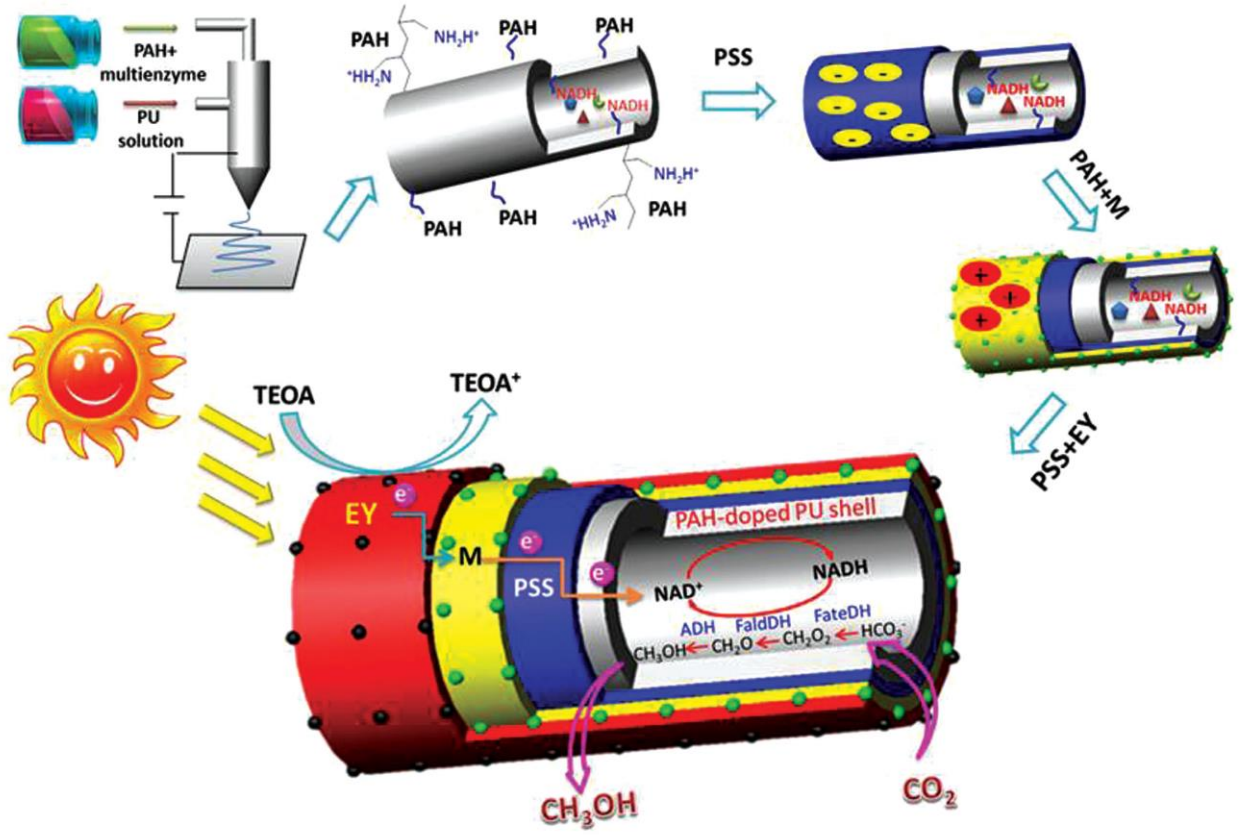


**Figure 5.** Schematic illustration of preparation of polyelectrolyte-doped hollow nanofibers/microcapsules-based integrated photosynthesis system for the solar-driven $CO_2$ transformation to methanol. Reproduced with permission from reference [53]. Copyright 2016 John Wiley & Sons.

Note that in different works, the co-immobilization of NADH with multi-enzymatic catalytic systems allowed to attend a higher methanol production efficiency over a single enzyme-based system. Furthermore, addition of photosensitisers, inorganic metal oxides and electron mediators as well as electron donors improved the photoreduction of $CO_2$ to methanol [53] [36].

**Table 2.** Methanol production from $CO_2$ using biomimetic photocatalysts

| **Photocatalytic system** | **Reaction conditions** | **$CH_3OH$ yield** | **Reference** |
|---|---|---|---|
| Sugarcane bagasse (SB) supported on graphitic carbon nitride (gCN) (SB-modified gCN) | $CO_2$ was purged through water bubbler and photocatalyst and irradiated for 12 h with 14 W LED | 110 µmol/g (g-SB-HT-E) 15-20 µmol/g (g-SB-HT-W) | [44] |
| Chitosan-$TiO_2$ | $CO_2$ was purged through water bubbler and photocatalyst and irradiated for 12 h with UV light | 0.37 nmol/g | [45] |
| Cuprous Oxide Nanoparticles Coated with Aminated Cellulose ($Cu_2O$/NCC-EDA) | $CO_2$ was purged through NaOH (120 mL of 0.5 mol $L^{-1}$) and photocatalyst (0.1 g) suspension and irradiated for 12 h with 300 W Xenon lamp | 1656.7 µmol/g | [54] |
| CuO/ ZnO-embedded carbohydrate polymer films (CuO/ZnO-Den-TOCNF) (CuO/ZnO-CS) | Catalyst Films were irradiated for 6 h with UV light at 5cm distance from the closed reactor bottle where water was dropped and dry ice (440–880 mg) was held | 0.030 mmol/g 0.037 mmol/g | [55] |
| Cu-loaded carbon modified titanium oxide (Cu-C/$TiO_2$). | NaOH (0.2 M) and catalyst suspension | 2600 µM | [46] |

| | | | |
|---|---|---|---|
| Carbon from glucose | was purged with $CO_2$ for 30 min and irradiated for 5 h with UV lamps | | |
| Tetraphenylporphyrin tetrasulfonate with methylviologen, triethanolamine and dehydrogenases ($H_2$TPPS/ $MV^{2+}$/TEOA/FDH/AldDH/ADH) | Suspension of $H_2$TPPS (100 μM), $MV^{2+}$ (2.0 mM), TEOA (0.3 M), FDH (2.0 μM), AldDH (2.0 μM) and ADH (2.0 μM) in $CO_2$ saturated 50mM sodium pyrophosphate buffer was irradiated for 100 min with 250W halogen lamp | 6.8 μM | [36] |
| Dehydrogenases (FDH/FalDH/ADH) encapsulated in hollow nanofibers and microcapsules | 10 mL buffer solution (50 mM PBS, pH 7.0), 15% (w/v) TEOA, 25 mg hollow nanofibers or microcapsules, 0.1 mg $mL^{-1}$ FateDH, 0.1 mg $mL^{-1}$ FaldDH, 0.1 mg $mL^{-1}$ ADH, 0.2 mM NADH, 0.25 mM M, and 50 μM EY irradiated for 10 h with 450 W Xenon lamp | 60.37 μM (hollow nanofibers) and 61.98 μM (microcapsules) 86.04% NADH photoregeneration | [53] |
| Chemically converted graphene | $CO_2$ (0.5 mL/min), β- | 11.21 μM | [52] |

| | | | |
|---|---|---|---|
| attached to isatin-porphyrin and coupled with dehydrogenases (CCG-IP/ FalDH/FDH/ADH) | $NAD^+$ (1.24 µmol), Rh (0.62 µmol), TEOA (1.24 mmol), photocatalyst (0.5 mg), 9 units of each enzyme (FDH, FalDH, and ADH) in 3.1 mL of sodium phosphate buffer (100 mM, pH 7.0) irradiated for 30 min with visible light | 38.99% NADH photoregenration | |
| Siliceous mesostructured cellular foams (MCF) functionalized with mercaptopropyl groups (MP) and co-immobilized with dehydrogenases (MFC-MP/FDH/ADH/FaldDH) | $CO_2$, MFC-MP, FateDH (0.05 mg $ml^{-1}$), FaldDH (0.75 mg $ml^{-1}$), ADH (3.75 mg $ml^{-1}$), NADH (100 mM), and $KHCO_3$ (200 mM) in 100 mM phosphate buffer (pH 6.5) | 1.35 mmol/g/min | [48] |

## 4. Biomimetic photocatalysts for the transformation of $CO_2$ to formic acid/formate

Formic acid (FA) also known as methanoic acid is a colourless, sour, pungent-smelling, and fuming liquid, with as chemical structure HCOOH. If this weak acid is toxic in case of skin and oral exposure, it is non-toxic and stable at room temperature conditions [56,57]. A variety of wood ants and bees produce large quantities of FA naturally, to protect their nest by spraying at prey [58]. FA is one of the most important chemicals as it has found application in a wide range of industries. It has been used for example as an anti-bacterial reagent, food additive, textile dyeing, leather tanning, rubber, finishing, drilling fluids, anti-icing, fragrance ingredient,

cleaning products, pH modifier, and corrosion inhibitor. It is also used as organic synthesis reagent in various industrial chemical processes [59–61].

Due to the high industrial demand for FA, its production at high scale crucial. Formerly, FA was produced as a by-product of acetic acid production through hydrocarbon oxidation which has been reduced after the implementation of the carbonylation of methanol method for acetic acid production. FA production was then fulfilled via hydrolysis of formamide, this method however was economically unfeasible due to the consumption of sulfuric acid and ammonia as well as ammonium sulfate formation [56]. Finally, the carbonylation of methanol followed by hydrolysis of methyl formate (**Eq. 5 and 6**) has been the main industrial process applied for FA production [62][63].

$$CH_3OH + CO \rightarrow HCO_2CH_3 \quad (5)$$

$$HCO_2CH_3 + H_2O \rightarrow HCOOH\,(FA) + CH_3OH \quad (6)$$

However, this conventional production process has encountered predicaments, being the work-up of the hydrolysis mixture the main issue. Also, in the course of separating unreacted methyl formate, re-esterification of FA and methanol to methyl formate happens very quickly due to the unfavourable equilibrium [64,65]. Finally, this conventional method has negative environmental impacts, and high energy and economic costs [66,67]. As a result, alternative ways of producing FA from other sources such as the reductive conversion of $CO_2$ are extensively researched [68–70]. Transformation of $CO_2$ to FA can significantly reduce carbon emissions and assist in fighting climate change whilst finding applications in hydrogen storage, chemical feedstock, and fuel in direct formic acid fuel cells (DFAFCs) [71][72]. Several methods allow the reduction of $CO_2$ to FA among which photochemical [73][74], electrochemical (ECR) [75][68], hydrogenation [69][76], and biological processes [77][78], stand a good position. The attractivity of the biomimetic photocatalytic transformation of $CO_2$ for FA production derives the abundance of biomaterials, environmental friendliness, and energy-saving to mention a few advantages. The mostly used biocatalyst is an enzyme, mainly the ᴅ-2-hydroxy acid dehydrogenase (FDH) that is found on methylotrophic microorganisms like bacteria and yeast that can use methanol. Tishkov and Popov reported that the FDH from bacterial sources exhibit 1.7 times higher activity than yeast [52]. The FDH enzyme catalyses the oxidation of formate to $CO_2$ and converts $NAD^+$ to NADH [79][80]. The cofactor β-nicotinamide adenine dinucleotide in its reduced form (NADH)

is normally needed by FDH enzymes to attain the reduction of $CO_2$ to HCOOH according to reaction (**Eq. 7**) below [81]. Around twenty studies that deal with the reduction of $CO_2$ into FA utilizing bio-based photocatalytic systems have been reported between 2012 and 2022 (see Table 3). These studies increased sharply from 2018 and exhibited promising conversion systems and high FA production yields.

$$CO_2 + NADH \leftrightarrow {}^{CbFDH}HCOO^- + NAD^+ \quad (7)$$

Yu et al. reported an effective and environmentally friendly light-driven enzymatic nanosystem [82]. This catalytic system consists of a combination between graphitic carbon nitride (g-$C_3N_4$) photocatalyst and two enzymes (carbon anhydrase (CA) and formate dehydrogenase (FateDH/FDH)), encapsulated in ZIF-8 MOF (CA&FateDH@ZIF-8/g-$C_3N_4$). **Fig. 6** illustrates the possible mechanism where photocatalytic NADH regeneration and enzymatic hydrolysis reduced $CO_2$ as described by the authors. Upon light irradiation, CA&FateDH@ZIF-8/g-$C_3N_4$ is excited to generate electron-hole pairs which then receive two electrons from the oxidation of one molecule of TEOA which are then excited from the valence band (VB) to the conduction band (CB) by light. The electron transport complex (M) was used to produce more 1,4-NADH, the biological entity needed by the enzymes. Thus, the highly selective M transports two electrons and one photon to $NAD^+$ for NADH regeneration. With the two enzymes, CA quickly converted $CO_2$ into $HCO_3^-$ which is converted into HCOOH using FateDH which, at the same time, consumes NADH as shown in Fig. 6. Reduction of $CO_2$ with CA&FateDH@ZIF-8/g-$C_3N_4$ system resulted in 198 µM of FA whilst the system without CA and free FateDH produced only 75 and 38 µM, respectively. When 2 $mg.mL^{-1}$ of CA&FateDH@ZIF-8/g-$C_3N_4$ was utilized, the optimized yield could reach 243 µM of FA. The activity of the enzymatic activity was retained above 80% after 10 runs, thus indicating the reusability of this catalytic system, that was also reported as able to shorten the distance between photocatalyst and enzyme entities, that is beneficial to the diffusion of substances and electrons.

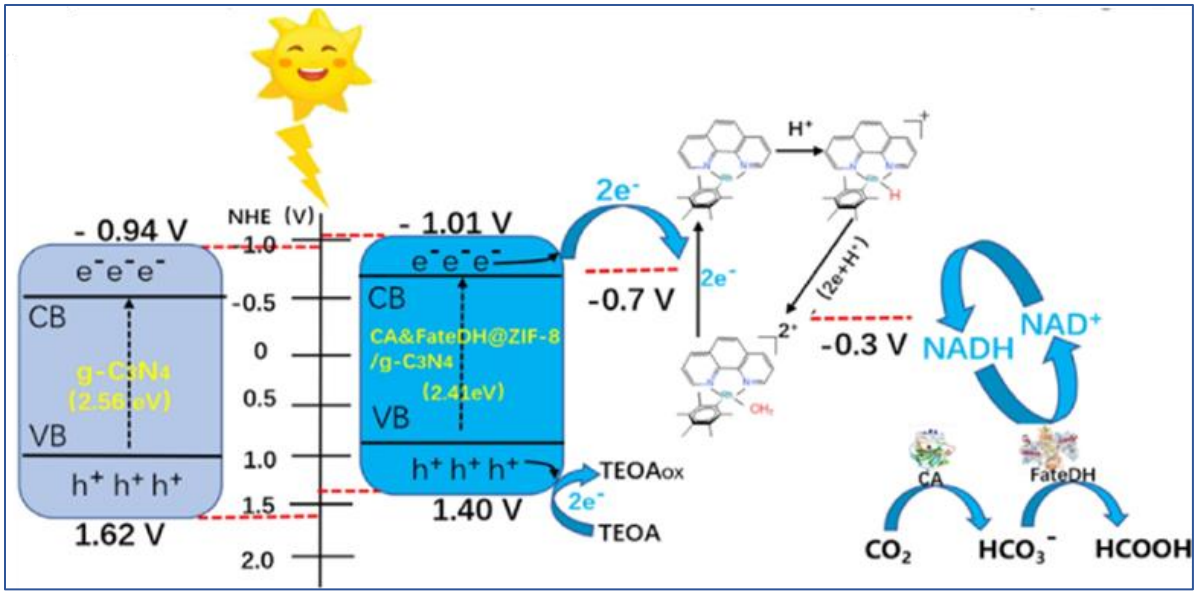


**Figure 6.** Illustration of electron and energy transfer processes for light-driven enzymatic CA&FateDH@ZIF-8/g-$C_3N_4$ nanosystem. Reproduced with permission from Reference [82]. Copyright 2021 Elsevier.

Wang et al. [83] reported a $CO_2$ reduction system consisting in two enzymes as well i.e. CA and FDH. Using a catalyst that combines two enzymes has been found to regulate the reaction rate and increase the loading amount of FDH which allows to decrease the ratio of of CA/FDH. This is one of the routes enhancing FA production. Sustaining a stable pH environment for this system in the course of $CO_2$ hydration was mandatory as the process releases hydrogen ions. The increase in the hydration rate of $CO_2$ increased the yield of FA by aspect of 4.2-fold. However, the costs of cofactor and enzymes are economically unfeasible and enzyme immobilization and cofactor regeneration appeared as a probable solution for low costs, recyclability, and enhanced biocatalyst stability.

A FDH-bearing hollow fiber membrane (HFM) reactor (**Fig. 7**) has been developed by Gu et al. [70] for $CO_2$ reduction which led to high-efficient and sustainable FA production. They used a UV-$TiO_2$ photocatalytic coenzyme regeneration system with a FDH-bearing HFM reactor which exhibited a maximum initial reaction rate of 1.04 $mM.h^{-1}$ and 81.7% yield. The optimization of operating conditions and NADH concentration provided a turnover number of 125 after 4.5 h. Considering that one mole of NADH is consumed to generate one mole of FA, NADH regeneration for continuous enzymatic production is important. Thus, the system regenerated

NADH when the reaction mixture was transported into a photocatalytic cell. This resulted in an instant regeneration of NADH which eventually showed that even at a low loading amount of NADH high FA production could be achieved.

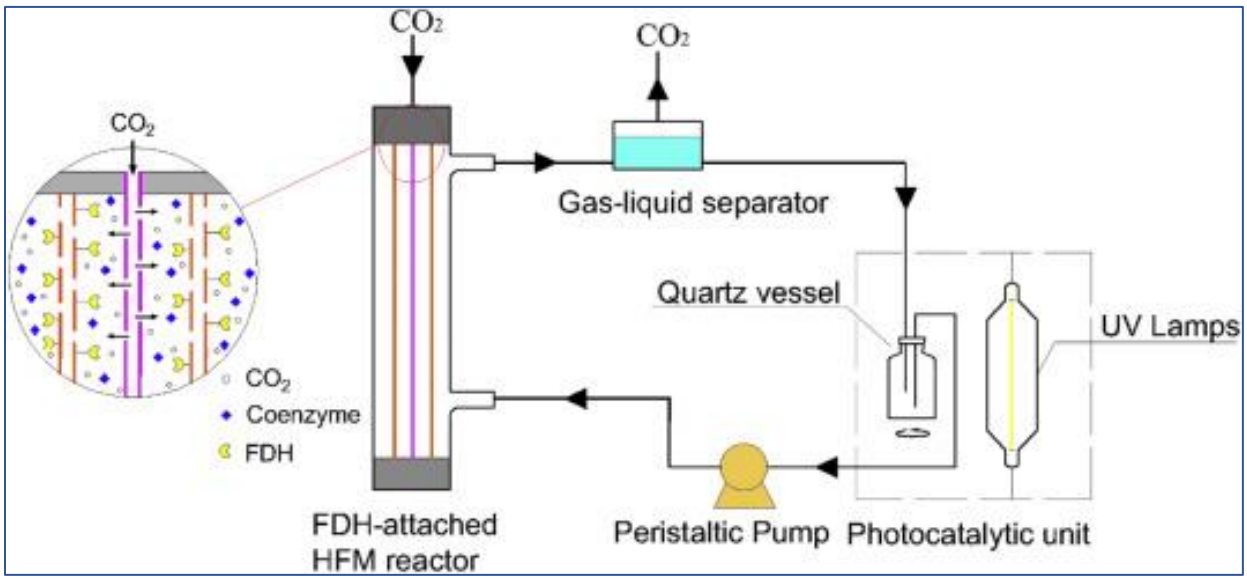


**Figure 7.** Illustration of a photocatalytic/enzymatic HFM system. Reproduced with permission from Reference [70]. Elsevier 2020.

Zhang et al. built an artificial thylakoid consisting of protamine-titania (PTi) micro-capsules with cadmium sulfide quantum dots (CdS QDs) and enzymes (FDH extracted from *Candida boidinii* (CbFDH)) for FA production from $CO_2$ [84]. The improvement of NADH regeneration activity ($4226\pm121$ $\mu molg^{-1}h^{-1}$) and enzyme compatibility of CdS/PTi microcapsules contributed to high FA production. Compartmentalization of photogenerated holes and reactive oxygen species (ROS) by the structure of CdS/PTi microcapsules protected FDH from deactivation, resulting in high compatibility between bio- and photo-catalyst. This catalytic system exhibited a quantum yield of $0.66\pm0.13\%$ of FA over multiple light-dark cycles.

Zhang et al. reported a highly selective reduction system with a metal-free heterojunction of pyromellitic diimide/g-$C_3N_4$ (PDI/CN) coupled with FDH enzyme [85]. **Fig. 8** shows the possible mechanism of the photoenzymatic catalytic cascade system on the PDI/CN heterojunction. In this cyclic process, the photocatalyst could continuously reduce $NAD^+$ to NADH while FDH could oxidize NADH to $NAD^+$, concurrently, in order to accelerate $CO_2$ transformation to FA. The process can successfully advance continual FA production. Another

study reported the utilization of $[Cp^*Rh(bpy)H_2O]^{2+}$ as a cocatalyst since the biologically inactive 1.6-NADH and the dimers of $NAD^+$ may be formed under the action of the intermediate radical. Thus, it was proven that $[Cp^*Rh(bpy)H_2O]^{2+}$ was effective for the selective production of biologically active 1,4-NADH [70]. Zhang et al. [85] have also shown herein the promoting effect of $[Cp^*Rh(bpy)H_2O]^{2+}$ in their system. The NADH yield increases linearly with the increase in sunlight irradiation time, and the system with $[Cp^*Rh(bpy)H_2O]^{2+}$ showed better performance signifying that this cocatalyst assists $NAD^+$ to accept photogenerated electrons thereby accelerating electron transfer to generate NADH. The outstanding performance of this photocatalytic system was ascribed to good conductivity, heterointerface effect, broad sunlight response range of the catalyst as well as a distinctive photoenzymatic catalytic cascade system. The system achieved 75% NADH yield and 114.8 μmol for FA production.

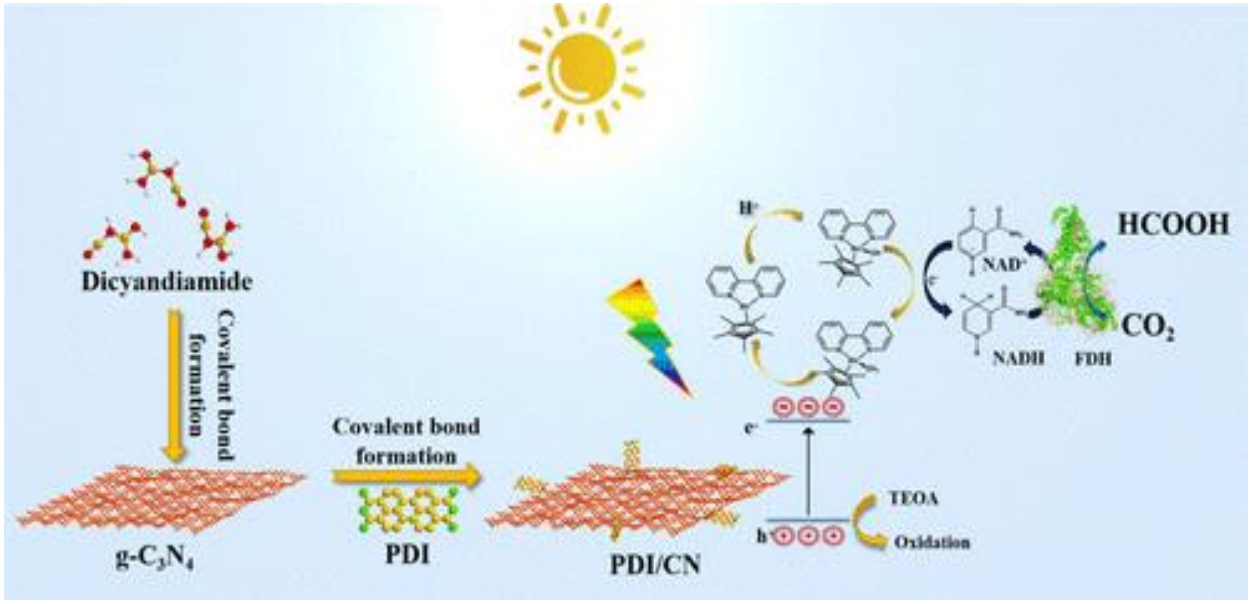


**Figure 8.** Possible mechanism of the photoenzymatic catalytic cascade system on the PDI/CN heterojunction. Reproduced with permission from Reference [85]. ACS Publications 2021.

Several studies concern the use of carbon-based materials such as carbon nanodots-silica hybrid, graphene film, graphene oxide modified with cobalt metallated aminoporphyrin, and $C_{60}$ polymer film as photocatalysts [86][33][87][34]. The interest in carbon materials emanates from their wide availability, environmental friendliness, and good light harvesting properties. Carbon nanodots were reported to have excellent biocompatibility, high solubility, and low toxicity whilst GO properties include biological function, thermal, mechanical, and biomedical [88].

Carbon nanodots-silica hybrid/FDH and graphene film/FDH systems showed NADH regeneration and FA yield of 74.10±0.17%, 203.33±1.9 μmol [86], and 71.8%, 228.6 μmol [33], respectively. For the FDH@GO-Co-ATPP system, NADH regeneration and FA yield of 48.53% and 96.49 μmol, respectively were reported [87] whilst the $C_{60}$-based polymeric/FDH system exhibited 91.07% of NADH regeneration and 239.46 μmol [34].

Ji et al. reported chloroplast-mimicking TCPP/$SiO_2$/Rh HNP-based wholly integrated APS and AM/M/BP HNS-based integrated Z-scheme APS models in 2018 [89] and 2020 [90]. These systems decreased the transfer distance of the energy and electron among the enzymatic redox and light-harvest system as well as enabling sufficient charge separation and photogenerated excitons transportation. In both studies, the effect of the TCPP/$SiO_2$/Rh HNPs and AM/M/BP HNS-based Z-scheme APS was confirmed by detecting photochemical, optical, and electrochemical properties. The TCPP/$SiO_2$/Rh HNPs system showed NADH regeneration which enhanced from 11 – 75% and FA production which increased from 10 – 100 μmol. AM/M/BP HNS-based Z-scheme APS, on the other hand, exhibited significant enhancement of NADH regeneration and FA production which reached 89% and 365 μmol, respectively [89][90].

The use of graphitic carbon nitride has been on the rise as well. This nitrogen-containing material possesses exceptional solar light-harvesting photocatalytic ability due to its slow recombination ability which increases photo-responsive energy transfer from the dye to a g-$C_3N_4$ moiety [91]. It has high stability, a tuneable band structure, strong visible light response, and astounding biocompatibility [92]. The systems reported by Cheng et al. [93], Zhang et al. [92], Singh et al. [91], and Kumar et al. [94] polymeric carbon nitride (PCN) mediated by a tannic acid/polyethyleneamine (TA/PEI), Rh complex $NH_2$-functionalized polymeric carbon nitride, 1-4,-diaminoanthaquinone monomer using a modified CN, and Se-doped CN nanosheets, respectively, showed FA production of 2.1 mM, 5.0 mM, 344.12 μmol, and 200.26 μmol.

Tian et al. [51] assembled a functionally compartmental inorganic photocatalyst-enzyme system that imitated chloroplast. Photoexcitation and enzymatic $CO_2$ reduction were compartmentalized by the thylakoid membrane with the purpose of protecting enzyme from photodamage whilst the system enables electron transfer thereby fostering photocatalyst. They built a tightly integrated artificial photosystem comprising of Rh complex cocatalyst onto thiophene-modified $C_3N_4$ (TPE-$C_3N_4$) and FDH encapsulated with MAF-7 which is a subclass of zeolitic imidazolate-

based MOF. The improved NADH regeneration of the system was attributed to the tightly integrated structure which promoted fast electron transfer from TPE-$C_3N_4$ to the Rh complex. MAF-7 not only protected FDH from photoinduced deactivation but also improved enzymatic stability in photosynthesis conditions. This photocatalytic system resulted in 16.75 mM FA after 9 h of illumination. **Table 3** shows the summary of the studies done on the transformation of $CO_2$ to FA using bio-inspired photocatalysts and the progress is promising.

**Table 3.** Biomimetic photocatalysts transformation of FA from $CO_2$.

| **Catalyst** | **Reaction conditions** | **Yield** | **Reference** |
|---|---|---|---|
| Bromophenol-Bakelite (BPB)/Rh complex/FHD | $NAD^+$ – 1.24 µM, BPB – 0.031 µM, AsA – 1.24 µM, Rh complex – 0.62 µM, sodium phosphate buffer – 3.1 mL | NADH regeneration – 82.52%<br>FA yield – 220 µmol | [95] |
| Bamboo-shape magnesium tetraphenyl porphyrin-based framework (Mg-TPPBF)/FDH | Photocatalyst – 15 µL in 3.1 mL of sodium phosphate buffer (100 mM, pH 7.0), β-$NAD^+$ – 124 µL, rhodium complex – 62 µL, FDH – 3 units, AsA – 310 µL | NADH regeneration – 73.9%<br>FA yield – 197.2 µmol in 2 h | [50] |
| 1,4-diaminoanthraquinone (AQ) monomer using a modified carbon nitride (CN) (AQBCN)/FDH | $NAD^+$/$NADP^+$ – 1.24 µmol, CpM – 0.62 µmol, AsA – 0.1 mmol, FDH – 3 units and the AQBCN photocatalyst – 0.5 mg in 3.1 mL of SPB (100 mM; pH, ~7.0) | NADH regeneration – 97.21/95%<br>FA – 344.12 µmol | [91] |
| Rh complex covalently grafted onto $NH_2$-functionalized polymeric | Photocatalyst – 12 mg, NAD – 120 µL, PBS – | NADH regeneration – | [92] |

| | | | |
|---|---|---|---|
| carbon nitride ($NH_2$-PCN) ($Rh_{m3}$-N-PCN)/FDH | 2.88 mL, FDH – 1 unit | 62.4%<br><br>FA yield – 5.0 mM | |
| CA&FateDH@ZIF-8/g-$C_3N_4$ | CA&FateDH@ZIF-8/g-$C_3N_4$ – 2 $mg.mL^{-1}$ in a 0.1 M PBS, TEOA – 10 w/v%, mediator – 1 $mg.mL^{-1}$, β-$NAD^+$ – 0.8 m | FA yield – 243 µM | [82] |
| Pyromellitic diimide/g-$C_3N_4$ (PDI/CN)/FDH | FDH – 3 units, catalyst – 10 mg, TEOA – 15 wt.%, phosphate buffer solution (pH 7.4, 100 mM) – 10 mL, β-$NAD^+$ – 0.1 mM, $[Cp^*Rh(bpy)-(H_2O)]^{2+}$ – 0.25 mM | NADH regeneration – 75%<br><br>FA yield – 114.8 µmol | [85] |
| Polymeric carbon nitride (PCN) mediated by a tannic acid/polyethyleneimine (TA/PEI) (PCN@TA/PEI-Rh core@shell)/FDH | Photocatalyst – 0.5 $mgmL^{-1}$, FDH – 2 $mgmL^{-1}$, $NAD^+$ – 1 mM, PBS buffer (pH 7.0, 100 mM), free Rh – 0.5 $mgmL^{-1}$, and $CO_2$ – 0.3 MPa. | NADH regeneration – 37.8%<br><br>FA yield – 2.1 mM | [93] |
| Covalent-organic framework/2,4,6-triformylresorcinol (COF-4)/FDH | Photocatalyst – 0.5 mg, β-$NAD^+$ – 1.24 mmol, AsA – 0.1 mmol, Rh complex – 0.62 mmol, and 3 units of FDH in 3.1 mL of 100 mM buffer (pH 7.0). $CO_2$ flow rate – 0.5 $mLmin^{-1}$ for 1 h in the absence of | NADH regeneration – 94.6%<br><br>FA yield – 226.3 µmol | [96] |

| | | | |
|---|---|---|---|
| | light | | |
| FDH@HFM/UV/$TiO_2$ | NADH – 2mM, liquid velocity – 40 $mL.min^{-1}$, gas velocity – 3 $mL.min^{-1}$ | FA yield – 81.7% | [70] |
| Antimonene/Cp∗Rh(phen)Cl/black phosphorus hybrid nanosheet-based Z-scheme (AM/M/BP HNS)/FDH | TEOA – 15 w/v%, AM NSs or BP NSs – 0.2 $mgmL^{-1}$, M – 0.1 mM, FDH – 0.3 units, $NAD^+$ – 0.1 mM | NADH regeneration – 35±4%<br>FA yield – 160±24 µmol | [90] |
| FDH@MAF-7/TPE-$C_3N_4$/PEI/Rh | $NAD^+$ g – 1 mM, phosphate buffer – 100 mM (pH 7), TEOA – 15 w/v%, MAF@FDH – 7.5 mg, TPE-$C_3N_4$/PEI/Rh – 3 mg | FA yield – 16.75 mM after 9 h<br>$5^{th}$ cycle FA – ~76% | [51] |
| FDH@Rh-NU-1006 | FDH@Rh-NU-1006 – $1.8\times10^{-3}$ M in Tris buffer (2 mL), TEOA – 0.5 mM, $NAD^+$ – 1 mM | FA yield – 0.144 ± 0.003 in 24 h | [97] |
| $C_{60}$-based polymeric system coupled with FDH enzyme | $CO_2$ flow rate – 0.5 $mLmin^{-1}$, β-$NAD^+$ – 1.24 µmol, TEOA – 1.24 mmol, 3 units of FDA in 3.1 mL of sodium phosphate buffer (pH 7.0, 100 mM) | NADH regeneration – 91.07%<br>FA yield – 239.46 µmol | [34] |
| CdS/TPi microcapsule-CbFDH | [$CO_2$] – 0.3 MPa, 37 ºC, visible light illumination (λ = 405±5 nm) | NADH regeneration – 93.03±3.84% | [84] |

| | | | |
|---|---|---|---|
| | $NAD^+$ – 5 nm, TEOA – 400 nm, CdS/PTi – 1 $gL^{-1}$, PBS buffer – pH 7.0, 100 nm, CbFDH – 1 $gL^{-1}$ | FA yield – 1500 $\mu Mh^{-1}$ | |
| FDH@GO-Co-ATPP | GO-Co-ATTP – 0.7 mg, $NAD^+$ – 1.24 mol, TEOA – – 1.24 mmol, 3 units of FDH in 3 ml of (100 mM, pH 7) sodium phosphate buffer | NADH regeneration – 48.53%<br>FA yield – 96.49 µmol | [87] |
| Porphyrin/$SiO_2$/Cp*Rh(bpy)Cl hybrid nanoparticles (TCPP/$SiO_2$/Rh-HNPs)/FDH | Phosphate buffer solution (100 mM, pH 7.0) – 10 mL, $NAD^+$ – 1 mM, TCPP – 0.5 mM, FDH – 0.3 units $mL^{-1}$, $CO_2$ – 0.3 MPa | NADH regeneration – 75%<br>FA yield – 100 µmol after 4 h. | [89] |
| Se-doped carbon nitride ($C_3N_4$) nanosheets/FDH | Photocatalyst – 0.5 mg, Rh – 0.62 µmol, β-$NAD^+$ – 1.24 µmol, FDH – 3 units, AsA – 0.1 mmol in 3.1 mL of sodium phosphate buffer (100 mM, pH 7.0)<br>$CO_2$ flow rate – 0.5 $mLmin^{-1}$ | NADH regeneration – 82.84%<br>FA yield – 200.26 µmol in 1 h | [94] |
| Graphene film photocatalyst (GFPC)/FDH | β–$NAD^+$ – 1.24 µmol, Rh complex – 0.62 µmol, FDH – 3 units in 3.1 mL of sodium phosphate buffer (100 mM, pH 7.0), AsA – 0.1 mmol, $CO_2$ | NADH regeneration – 71.8%<br>FA yield – 228.6 µmol in 2 h | [33] |

| | | | |
|---|---|---|---|
| | flow rate – 0.5 $mLmin^{-1}$ | | |
| Carbon nanodots-silica hybrid (CNDSH)/FDH | Photocatalyst – 0.5 mg, β-$NAD^+$ – 1.24 mmol, rhodium complex – 0.62 mmol, ascorbic acid – 0.1 mmol, FDH – 3 units in 3.1 mL of $Na_2HPO_4$-$NaH_2PO_4$ buffer (100 mM, pH 7.0) | NADH regeneration – 74.10±0.17%<br>FA yield – 203.33±1.9 µmol | [86] |
| Cobaloxime/eosin/REOA/FDH | Eosin Y – 0.10 mM, $NAD^+$ – 0.50 mM, TEOA – 0.20 M, 5 units of FDH in 0.15 M phosphate buffer (pH 7.0) | FA yield – 36% | [98] |

## 5. Biomimetic photocatalyts for the transformation of $CO_2$ to acetic acid

Acetic acid otherwise known as vinegar acid, ethanoic acid and methane carboxylic acid is a clear, colourless liquid, of pungent smell and with the chemical formula $CH_3COOH$. It is the second simplest carboxylic acid after formic acid and is of high importance also due to a plethora of industrial and pharmaceutical applications. It is produced synthetically and it can also be prepared via bacterial fermentation. It is a crucial chemical reagent being primarily used for the production of cellulose acetate for photographic films and that of acetic anhydride. Acetic acid also possesses antiseptic properties, so it can be employed as antimicrobial agent. The current approach for the production of acetic acid is not environmental benign, with high energy cost and the production scale cannot meet the demand for both industrial and pharmaceutical needs [99,100]. Development of alternative production routes that will cover the current demand and be environmentally friendly is thus needed. One of the promising and cost-effective methods to produce acetic acid is the photocatalytic transformation of $CO_2$. Recent advancements in this domain are described below but note that only a few of case studies were found in the literature of the last decade.

Zhang and co-authors [12] integrated ultra-small gold nanoclusters (AuNCs) and cadmium sulfide (CdS) into M. thermoacetica bacteria and compared their performance in the photosynthesis of acetic acid from $CO_2$ (**Fig. 9a**). These bio-based photocatalytic systems were found efficient for $CO_2$ fixation into acetic acid under low light irradiation and dark (**Fig. 9b**). The authors observed that the yield in acetic acid by the gold-based biophotocatalyst after four days is conspicuously higher than that obtained with cadmium sulfide-based bio-photocatalyst under the irradiation of low light. Moreover, the authors found that the activity of ordinary bacterium (M. thermoacetica) and gold-based bio-photocatalyst in darkness are relatively low. A monitoring of the electron transfer mechanism via photoluminescence confirmed that the photo-excited electrons from the gold nanoclusters are migrated to distributed redox mediators in the bacteria cytoplasm such as flavoproteins. Evaluation of the effect of cysteine on the yield of acetic acid production revealed that the gold-based bio-photocatalyst produced the highest yield (6.01 $mmolg^{-1}$) at 0.3 % wt Cys. It is worth to mention that the ligands at the gold nanoclusters surface and the gold core size can be changed in order to tune their biochemical and biophysical characteristics, including cell uptake, cytotoxicity, biocompatibility, and molecular electronic structures. This study demonstrated that integration of gold nanoclusters as intercellular photosensitizer inside the cytoplasm of M. thermoacetica bacterium allowed this non-photosynthetic latter to conduct effective photosynthesis of acetic acid from $CO_2$.

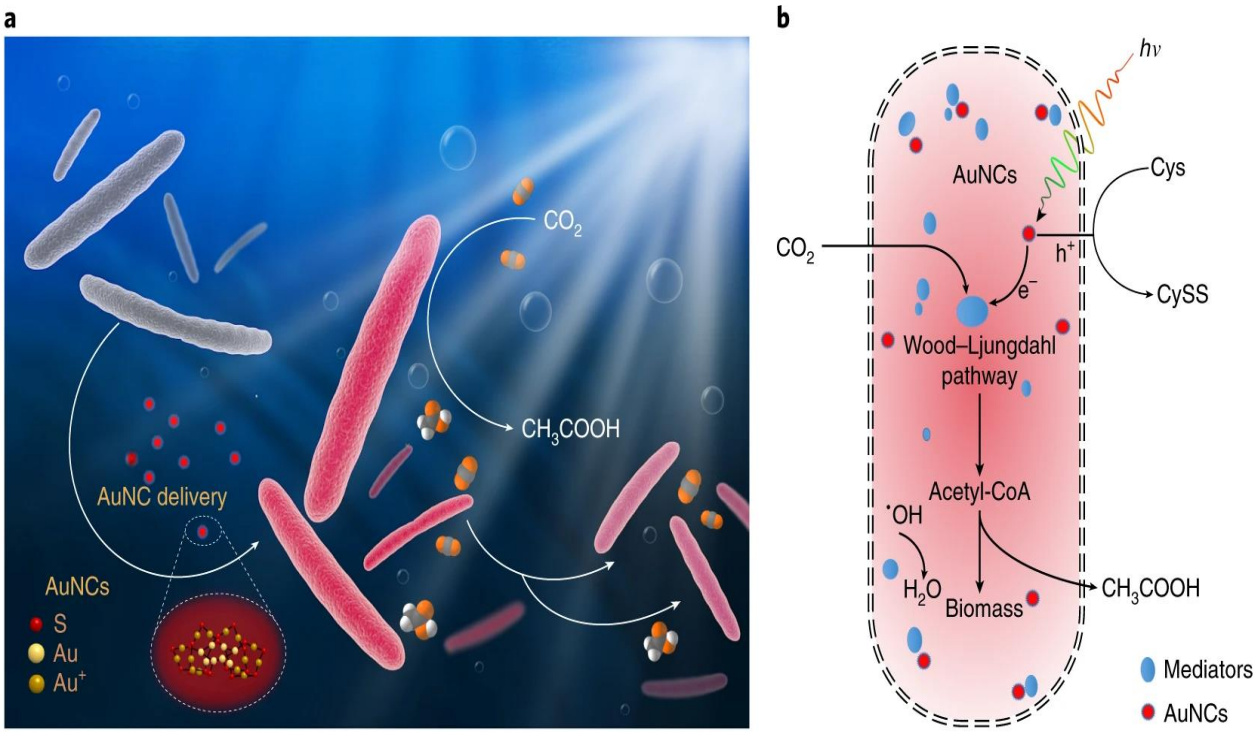


**Figure 9** (a) Schematic illustration of *M. thermoacetica*/AuNCs hybrid system (b) Schematic bacteria electron transfer pathway for acetic acid generation under illumination of light

In another study, Gai et al. [101] developed an organic semiconductor – bacteria biohybrid photosynthetic system that efficiently conversed $CO_2$ into acetic acid. The bacterium involved is Moorella thermoacetica whose surface was coated with perylene diimide derivative (PDI) and poly(fluorene-co-phenylene) (PFP) as photosensitizers. This led to the formation of a p-n heterojunction (PFP/PDI) layer with high hole/electron separation efficiency (**Fig. 10**). The π-conjugated semiconductors display excellent light-harvesting ability and biocompatibility. In addition, the cationic side chains of the two organic semiconductors could intercalate into cell membranes, thus allowing an efficient transfer of electrons to the bacterium. In this photocatalytic system, the bacterium could harvest photoexcited electrons from the PFP/PDI heterojunction and synthesize acetic acid from $CO_2$ under illumination. This bio-photocatalytic system showed an efficiency rate of 1.6% which is comparable to those of reported inorganic biohybrid systems.

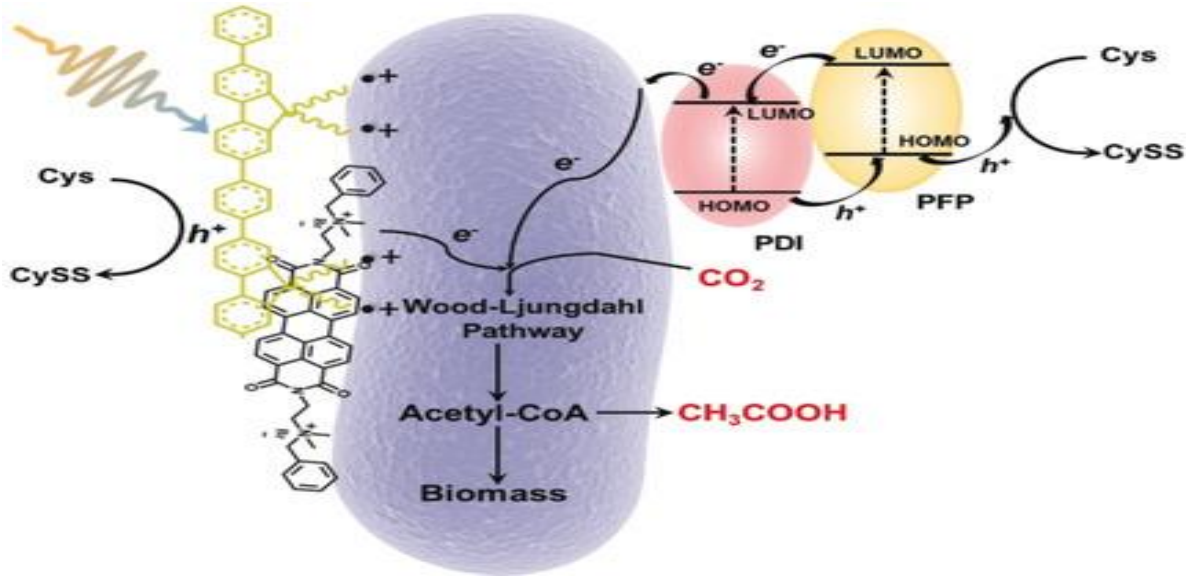


**Figure 10.** Wood–Ljungdahl pathway for $CO_2$ reduction in the presence of PFP/PDI/M. thermoacetica. Reproduced with the permission from [101].Copyright 2020 Willey online

Tharak and colleagues [102] reported microbial-mediated $CO_2$ in gas and gas-electro fermentation systems with and without applied potential by selectively enriched biocatalysts (**Fig. 11**). In the Heat + $CO_2$ condition during the gas fermentation (GF) stage, the maximum production was 0.84 g/L acetic acid with 31 $mg.L^{-1}.h^{-1}$ inorganic carbon fixation rate (ICFR). The GF was tested in a single-chambered microbial electrochemical system (MES; Gas-electro fermentation) at different applied potentials (-0.4 and -0.6 V vs Ag/AgCl [3.5 M KCl]). With -0.6 V applied potential, a higher acetic acid production of 1.02 g/L was obtained. The $CO_2$ fermentation efficiencies were improved by higher charge transfer rates (52% faradaic efficiency) and lower corrosion and resistances (Rct -0.4 ohm). On continuous conditions, an abundance of Proteobacteria, Firmicutes, and Actinobacteria in the enriched biocatalyst represented a significant shift of the microbiome towards $CO_2$ feeding microbes.

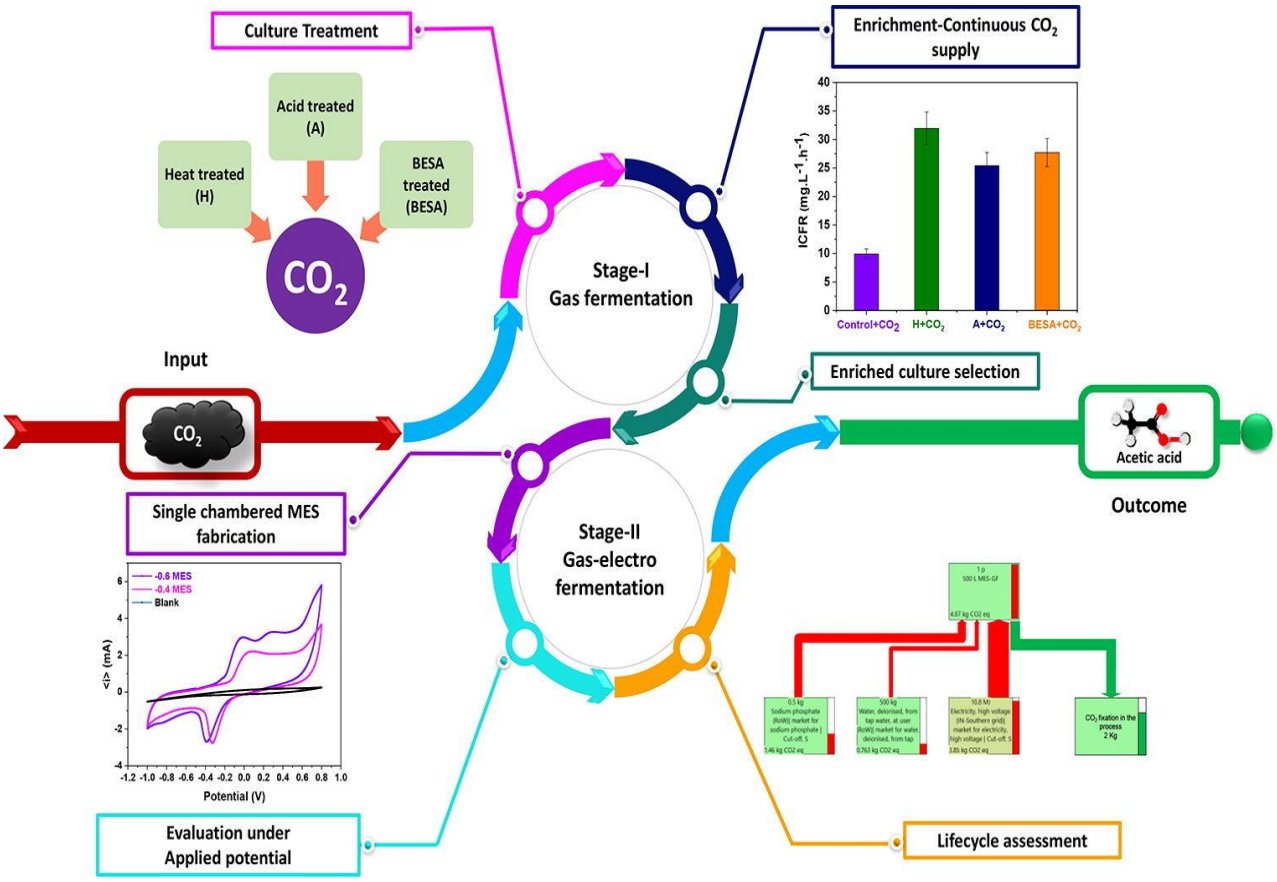


Fig. 11. Schematic diagram of acetic acid production from $CO_2$ via lignin/ionic based catalytic system. Reproduced with the permission from [102]. Copyright 2023 Elsevier

Wang and co-workers [103] reported a new strategy to produce renewably sourced acetic acid from lignin and $CO_2/H_2$. The catalytic system is based on an ionic liquid (that is 1- butyl-3-methylimidazolium chloride, [BMIm][Cl]) that contains a Ru-Rh bimetal catalyst ($Ru_3(CO)_{12}$ and $RhI_3$) and Li salt additives (LiI and $LiBF_4$). This system was effective for the production of acetic acid in the temperature range of 120-180 ℃ under low pressure of $CO_2$ (1 MPa), affording an acetic acid yield of 94% at 180 ℃. In addition, taking lignin as the feedstock, 0.17 g of acetic acid was produced from 1 g of lignin. Finally, the catalytic system could be recycled 5 times without decrease in performance. Investigation of the reaction mechanism evidenced that lignin provided methyl group to form $CH_3I$, while the $[BMIm]^+$ -stabilized $RhI_3$ and $I^-$-complexed $Ru(CO)_{n(n=1\sim4)}$ cooperated and catalyzed the formation of acetic acid from $CH_3I$ and $CO_2/H_2$.

**Table 4** below summarizes the biomimetic materials explored for the production of acetic acid. While there is appreciable development towards the production of acetic acid from $CO_2$ using

biomimetic materials, the yields reported are very low and cannot satisfy the commercial purpose. This calls for more research efforts in this hot topic.

Table 4. Biomimetic photocatalysts for acetic acid production from $CO_2$

| Photocatalystic system | Reaction conditions | Yield | Reference |
|---|---|---|---|
| M. thermoacetica/AuNCs hybrid system | Low-intensity simulated sunlight (calibrated by photodiode, air mass 1.5 global spectrum (AM 1.5), $2Wm^{-2}$ ) | 6.01 $mmolg^{-1}$ after six days in the presence of cysteine as sacrificial agent | [12] |
| M. thermoacetica/CdSNPs hybrid | Air mass 1.5 global spectrum, 2 W $m^{-2}$, photons; 5 x $10^{13}$ $cm^{-2}$ $s^{-1}$ under light and dark flux at $\lambda$ = 435 to 485 nm | 85±12% quantum yield after four days | [104] |
| PFP/PDI/M. thermoacetica p-n heterojunction | 5.0 $Mw/cm^2$ power density, under of light-dark cycle for 12h | 0.1 mM in dark, 0.6 mM under light | [101] |
| Different bacteria mediated biocomposites | Heat-shock, Acid-shock and 2-Bromoethano sulphonate (BESA), 31 mg $L^{-1}$ $h^{-1}$ of ICFR, (-0.4 and -0.6 V vs Ag/AgCl [3.5 M KCl]), $R_{ct}$ = 0.4 ohms | 1.02 g/L at 52% FE | [102] |
| Lignin/ionic based catalytic system | 180 ℃, 1 MPa | 94% yield, 0.17g acetic acid produced from 1g of lignin | [103] |

PFP: poly(fluorene-co-phenylene), PDI: perylene diimide derivative, FE: Faradaic efficiency, ICFR: Inorganic carbon fixation rate

## 6. Mechanistic insights of biomimetic photocatalysts for $CO_2$ Reduction

There is no definite mechanism for the reduction of $CO_2$ as it is a complex reaction involving radicals, electrons, and protons [105]. Generally, after the reduction of $CO_2$ by a one-electron transfer and the formation of surface-bound $CO_2^{\cdot-}$, the process proceeds through a sequence of elementary steps involving the transfer of a proton, electron or radical ($H^{\cdot}$), as well as breaking C-O bonds and creating C-H bonds. Several intermediates are radical species, partially accounting for the number of possible pathways and final products at different stages of recombination. The exact sequence and mechanistic flow of each subsequent step have not been thoroughly elucidated, but some literature suggests that photocatalytic reduction of $CO_2$ *via* biocatalysis has a similar pathway than that described for transition metal photocatalysis [105].

Hydrogen radicals ($H^{\cdot}$) bind to the oxygen atom of the adsorbed carboxyl radicals ($CO_2^{\cdot-}$), resulting in an immediate cleavage of the C-O bond, subsequently leading to the formation of carbon monoxide. In a separate mechanism, the carboxyl radicals recombine with hydrogen radical to form formic acid. In a next step, formic acid accepts another hydrogen radical to form a dihydroxymethyl radical, which is dehydrated when another hydrogen radical is attached to the formaldehyde. Two additional steps of reduction lead to $CH_3OH$ formation, which is further reduced to methane in two more steps of reduction. A proposed mechanistic pathway (by formaldehyde, carbene, glycol pathways) for the reduction of $CO_2$ to CO, formic acid, and methanol as described in the literature is presented in **Fig. 12** [106].

Formaldehyde pathway

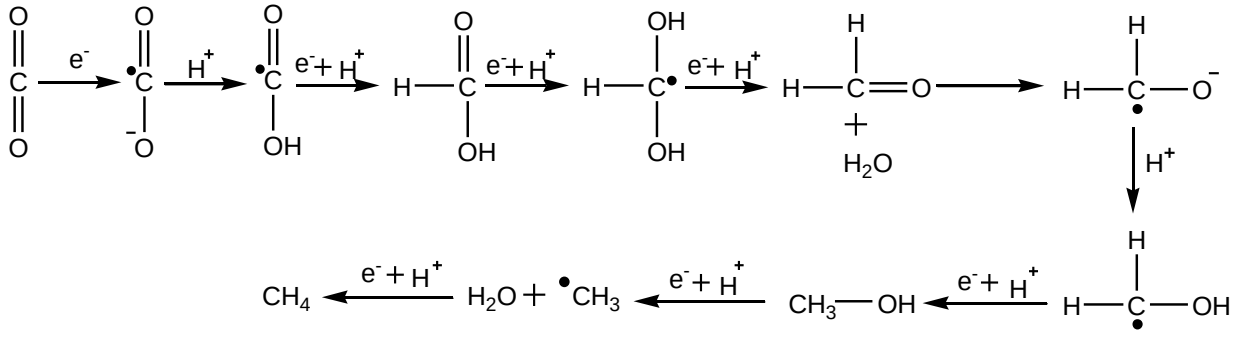

Carbene pathway

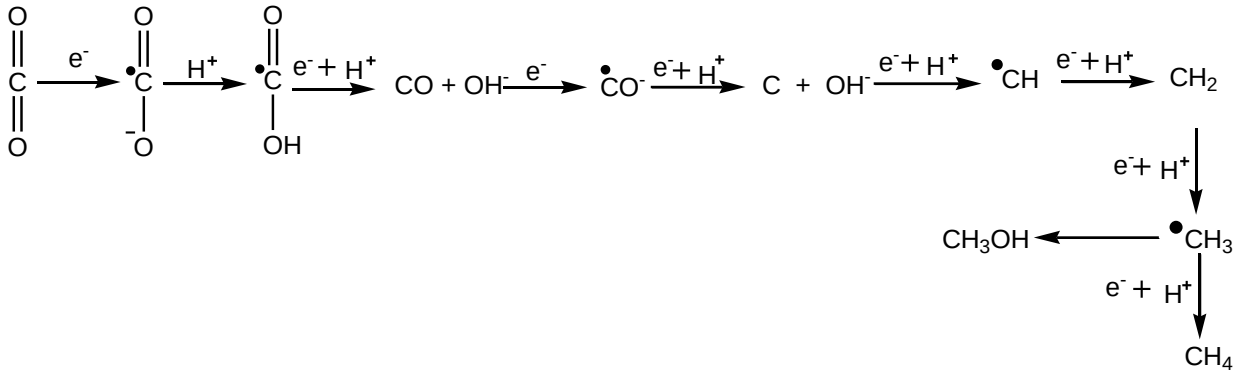


**Figure 12.** Two reduction routes for $CO_2$; top, formaldehyde pathway and bottom carbene pathway [106].

The mechanism of $CO_2$ conversion involves two-electron reduction mediated by metal-based catalysts or enzymes. Most photocatalysts are metal-based [107][108][109][110][111]. For a commonly described metal photocatalyst, the semiconductor part absorbs photon energy, which leads to the excitation of electrons from valence band (VB) to conduction band (CB), creating electron−hole pair. The holes in VB have strong oxidizing ability, especially for water oxidation and electrons in CB reduce $CO_2$. Water oxidation produces hydrogen ions and hydroxyl radicals, and the activated $CO_2$ reacts with excited electrons and hydrogen ions, which finally result in the formation of formic acid, formaldehyde, and methanol [112]. When $AgCuInS_2$ supported on graphene-$TiO_2$ are parallelly activated, electrons transfer through the graphene to reach the VB of $TiO_2$ to form the donor level, thus, resulting in the formation of photogenerated electrons ($e^-$) and holes ($h^+$) at the active sites of $AgCuInS_2$ photocatalyst. The holes ($h^+$) react with the adsorbed $2H_2O$ to produce oxygen ($O_2$), electron ($e^-$) and protons ($H^+$). Surface-adsorbed $CO_2^{\bullet-}$ radical generated by the injection of a single electron reacts with $e^-$ and $H^+$, producing CO, which undergoes a further reduction process forming the surface-adsorbed C. $CO_2$ further reacts with excited electrons ($2e^-$) and hydrogen ions ($2H^+$) to yield HCOOH. The further reaction of HCOOH with excited electrons ($2e^-$) and hydrogen ions ($2H^+$) led to a loss of water ($H_2O$) to produce an intermediate, formaldehyde, (HCOH) (typical of formaldehyde pathway, see Fig 11). Surface adsorbed formaldehyde reacts with $2e^-$ and $2H^+$ to yield methanol as a main product. A schematic representation of photocatalytic $CO_2$ reduction process with $AgCuInS_2$ is illustrated in **Fig. 13**.

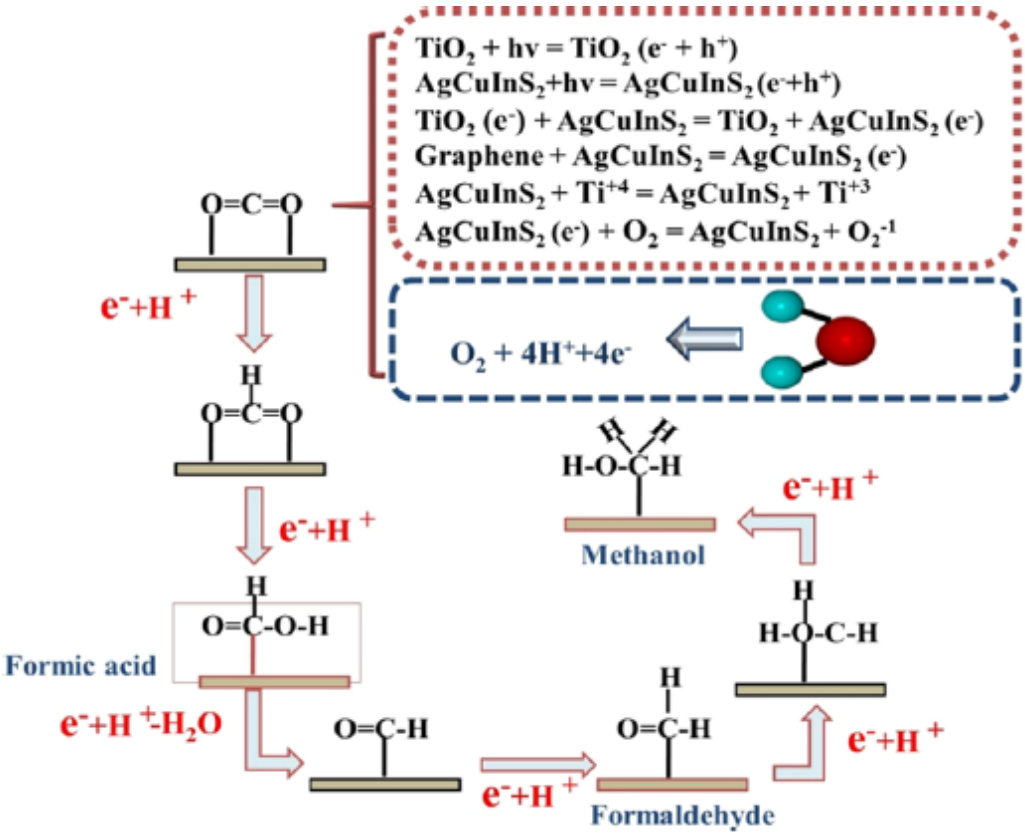


**Figure 13.** Schematic diagram of the photocatalytic $CO_2$ reduction process. Re-used with permission from. Copyright (2021) American Chemical Society. [112]

Getahun et al. [55] concerned the use of metal oxides (ZnO and CuO) embedded with bio-based materials (such as chitosan) as photocatalysts. Both ZnO and CuO absorb UV light, making energy separation to occur, and resulting in hydrogen ion ($H^+$) and electron ($e^-$) generation. The schematic representation of photocatalytic $CO_2$ reduction using ZnO and CuO under UV light is illustrated in **Fig. 14**. The valence-band energy level of CuO (n-type) is higher than that of ZnO (p-type), the holes of ZnO generated by absorbing light energy transfers to the valence-band level of CuO, leading to the holes ($h^+$) on CuO/ZnO composite oxidizing water ($H_2O$) to oxygen ($O_2$), hydrogen ion ($H^+$) and an electron ($e^-$). $CO_2$ (trapped within amine groups of chitosan and dendrimer, $-NH_2---CO_2$) reacts with $e^-$ to form anion radical $CO_2^{\bullet-}$ (a single electron reduction of $CO_2$) followed by a reaction with protons $H^+$, a process known as "proton-assisted multielectron reduction". Surface-adsorbed $CO_2^{\bullet-}$ radical reacted with $6e^-$ and $6H^+$ ($CO_2 + 6H^+ + 6e^- \rightarrow CH_3OH + H_2O$), producing methanol. Therefore, the photoredox pathway could be considered a

proton-assisted multielectron reduction via the formaldehyde route. Pathway for CO and formic acid production are similar to those reported by Otgonbayar et al [110].

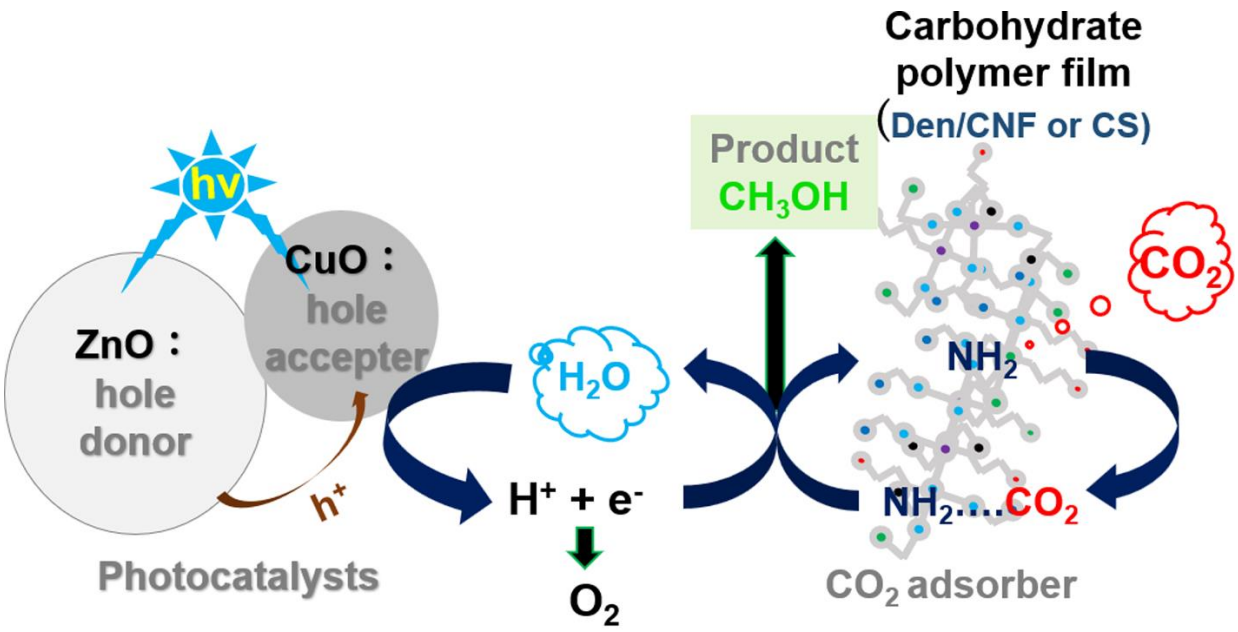


$$2H_2O \rightarrow 4H^+ + 4e^- + O_2$$

$$-H_2N\cdot\cdot\cdot CO_2 + 6H^+ + 6e^- \rightarrow -NH_2 + CH_3OH + H_2O$$

**Figure 14.** Illustration of $CO_2$ photocatalytic reduction to methanol with $H_2O$ oxidation on films of CuO/ZnO catalytic-embedded carbohydrate polymer. Reproduced with permission from [55]. Copy rights (2022) Elsevier.

The photocatalytic reaction mechanism of metal-based systems are similar to those followed by enzymes such as carbon monoxide dehydrogenases (CODHs) [113] and formate dehydrogenases (FDHs) [114][115], in which two to four electron reduction of $CO_2$ is required for conversion to carbon monoxide, formic acid/formate, and methanol. The bio-inspired mechanistic insight for two-electron reduction of $CO_2$ to CO, as described by Mondal et al, 2014 [105] goes through proton-coupled electron transfer (PCET, $H^+ + e^-$), from a molecule that acts as "electron and proton" donor (reductant) to another one that acts as an acceptor (oxidant). Both biocatalysis and homogeneous transition-metal catalysis usually proceed *via* redox reaction where hydride transfer takes place for formate ion production (**Fig. 15**).

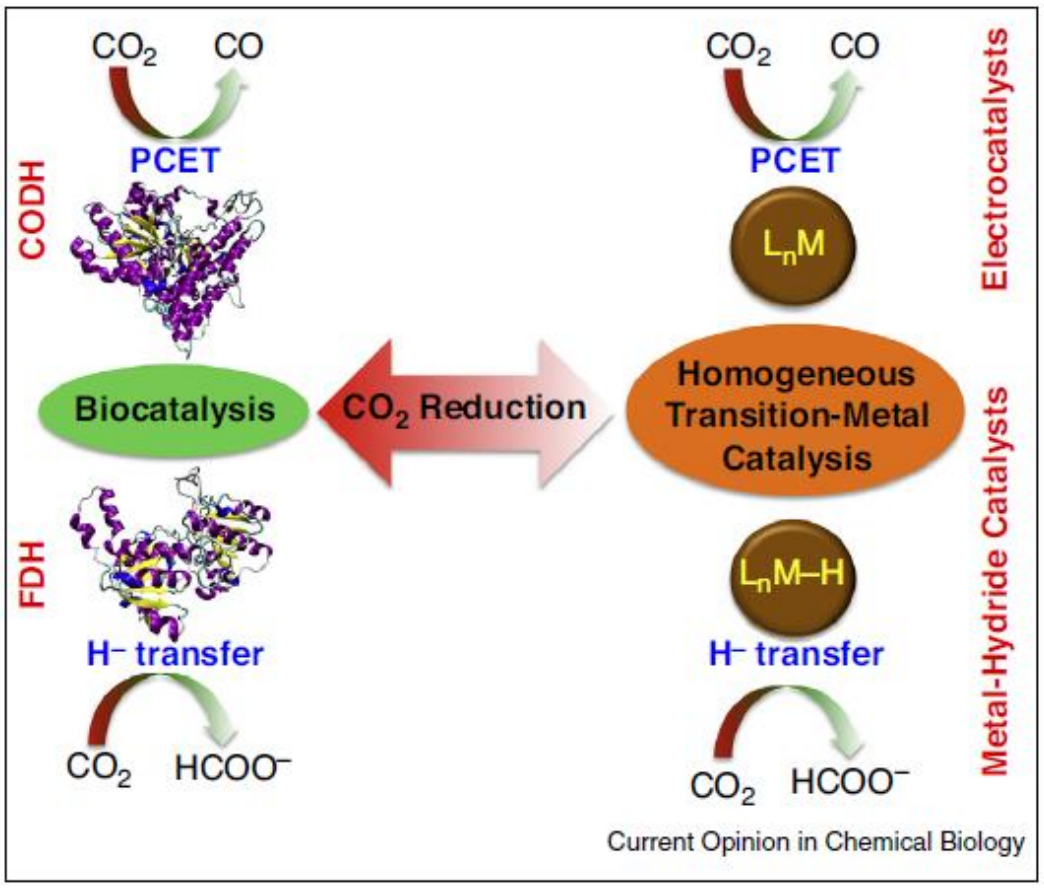


**Figure 15.** Overview of the bio-inspired mechanistic insight into the two-electron reduction of $CO_2$ to CO and FA (PCET = proton-coupled electron transfer). Copyright [105].

FDHs are known to catalyze the reduction of $CO_2$ to formic acid through a proton ($H^+$) transfer mechanism ($CO_2 + NADH + H^+ \leftrightarrow HCOOH + NAD^+$) as well as reversible oxidation of formate to $CO_2$ ($HCOO^- \leftrightarrow CO_2 + H^+ + 2e^-$) [114][116][117]. β-Nicotinamide adenine dinucleotide hydrate reduced salt (NADH) is an essential co-factor for FDH, its efficiency is highly dependent on the NADH concentration as a hydrogen donor. $NAD^+$ is the oxidized form of β-Nicotinamide adenine dinucleotide hydrate (NAD). The active site of the $NAD^+$-based FDH showing the C4-atom position on pyridine ring (**Fig. 16a**). Mondal et al., [105] reported the direct hydride transfer, occurs from the C-atom of the formate to the C4-atom of pyridine ring of $NAD^+$, leading to NADH and $CO_2$ (**Fig. 16b**). The neighbouring residues on FDH such as Thr (Thr282), Asp (Asp308), Ser (Ser334) and Gly (Gly335) interact with the positively charged $NAD^+$ ring and stabilize it, thereby promoting the hydride transfer from formate to C4 [118][119][120].

Generally, enzymatic reduction of $CO_2$ usually proceeds to $HCO_2^-$, and the oxidized form of nicotinamide cofactor ($NAD^+$) is reduced to NADH by glutamate dehydrogenase (GDH).

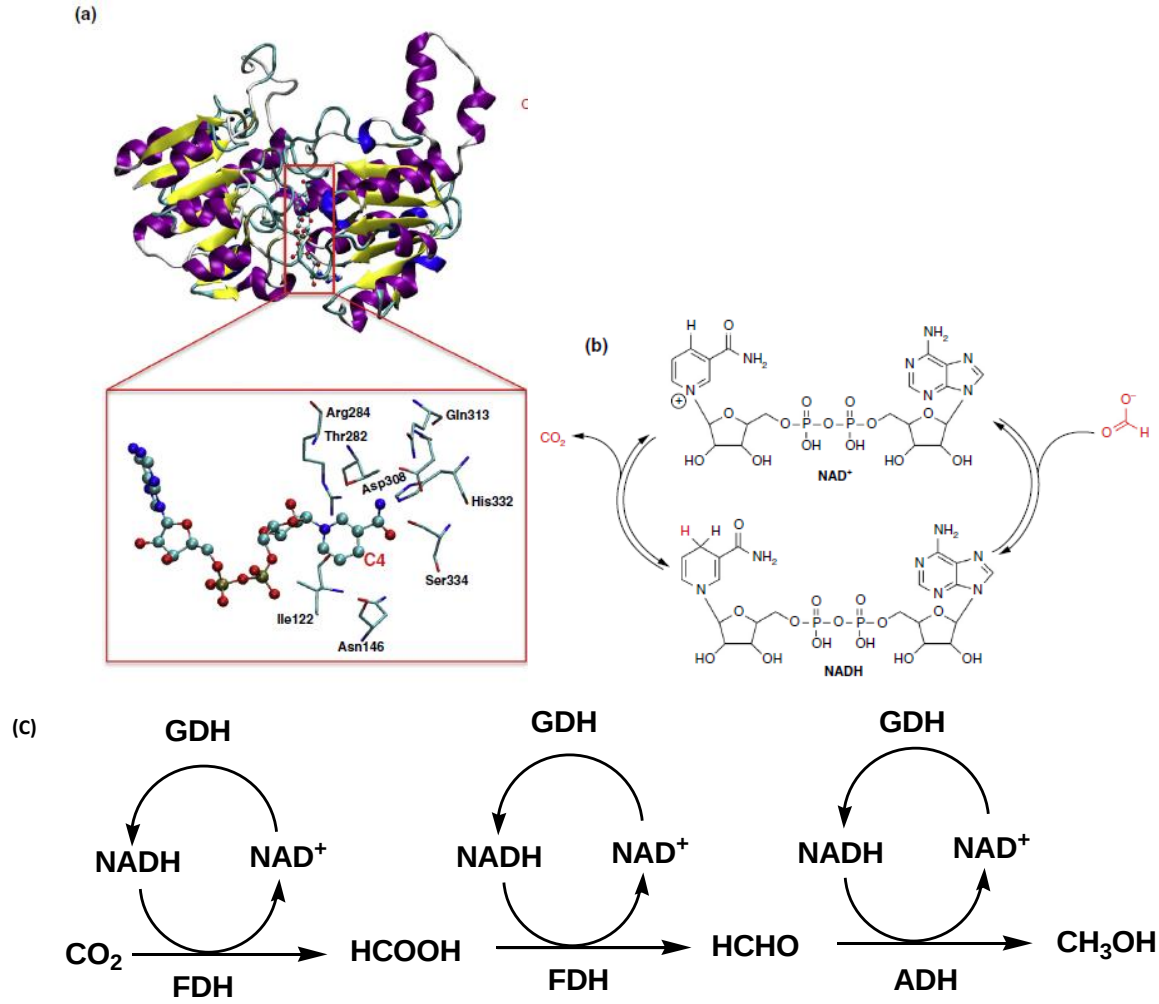


**Figure 16.** Two-electron reduction of $CO_2$ to HCOOH; (a) the active site of the $NAD^+$-based FDH, (b) the catalytic mechanism of FDH Copyright [105], (c) a simplified reaction pathway of $CO_2$ to methanol (FDH, formaldehyde dehydrogenase (FDH), alcohol dehydrogenase (ADH)). The regeneration of NADH was catalyzed by glutamate dehydrogenase (GDH) [114].

A complex system of enzymes such as adenosine triphosphate (ATP), guanosine triphosphate (GTP), nicotinamide adenine dinucleotide (NAD or NADH for the reduced form), or nicotinamide adenine dinucleotide phosphate (NADP or NADPH for the reduced form), working in tandem is vital when considering biological conversion of $CO_2$. There is a need to further

research in this area especially around the regeneration of cofactor NADH, which in turn, improves enzyme efficiency during complex $CO_2$ bioprocessing applications.

In the formation of acetic acid, methanol carbonylation is required, and the reaction comes after the formation of Methanol (photocatalytic reduction of $CO_2$) [101] by using metals catalysts such as gold, platinum, palladium, osmium, copper-nickel, copper-Mordenite, palladium-cerium, ruthenium, rhodium, and lanthanum. Metal complexes play a huge role in achieving the carbonylation reaction through formation. In a typical $Rh/CH_3I$ catalysed system, a series of activated anionic species such as cis-$[Rh(CO)_2I_2]^-$, $[(CH_3CO)\text{-}Rh(CO)I_3]^-$ and $[(CH_3CO)\text{-}Rh(CO)_2I_3]^-$ to assist with product formation. Halogen additives is required to promote the reaction by activating C-O bond in methanol and on transition metal complexes to form methyl iodide (**Eq. 1**) which reacts with carbon monoxide to form acetyl-iodide (**Eq. 2**) and can quickly reach acetic acid final product when hydrolyzed in water (**Eq. 3**). The metal catalyst is recycled at the end of the reaction.

$$CH_3OH + HI \rightarrow CH_3I + H_2O \quad (\mathbf{1})$$

$$CH_3I + CO \rightarrow CH_3COOI \quad (\mathbf{2})$$

$$CH_3COOH + H_2O \rightarrow CH_3COOH + HI \quad (\mathbf{3})$$

**Conclusion and perspectives**

The potential of using bio-based photocatalysts for the conversion of $CO_2$ into value-added products, has been emphasized by describing the main advances in this domain from the literature in the last decade. The investigation of such catalytic systems is fundamental as this may afford the development of environmentally friendly, and sustainable processes as alternatives to replace the use of fossil fuels and consequently, contribute to the decrease global warming. The reported bio-inspired photocatalytic systems are presented following the target chemicals, namely carbon monoxide, formic acid, methanol and acetic acid (via carbonylation of methanol) all being key chemicals for a direct use in various applications or as intermediate synthons. Several case studies concern the use of metal catalysts combined with biomaterials which, under photocatalytic conditions, allow the formation of $CO_2$-derived carbon molecules. The reduction of $CO_2$ using bioinspired catalysts is generally accompanied by proton-coupled

electron transfer (PCET) resulting in C–O bond cleavage to yield CO, an initial carbon-based product. $CO_2$ conversion to formic acid is usually promoted by formate dehydrogenase (FDH) and its co-factor NADH, responsible for donating hydrogen [117][118]. Carbonic anhydrase one of the fastest enzymes that catalyses $CO_2$-hydration reaction has been combined with formate dehydrogenase (FDH) with co-factor NADH to form formate/formic acid [119][122][121][119]. One of the major drawbacks is the depletion of NADH during catalytic reduction reaction to $NAD^+$, thus requiring continuous regeneration to NADH to have sustained formic acid production. The enzymes used for conversion of $CO_2$ to $CH_3OH$ are Formate Dehydrogenase (FDH) that utilizes NADH as a cofactor, and alcohol dehydrogenase (ADH). Enzymes usually exhibit much reduced activities over time due to impurities, slight change in reaction condition, (such as pH and temperature). The presence of transition metal/metal oxides incorporated unto biopolymers and enzymes facilitate the reduction of $CO_2$ to various products by promoting metal-$CO_2$ interaction. An example is [NiFe] CO Dehydrogenase ([NiFe] CODH), an enzyme used for conversion of $CO_2$ to CO. Zinc complexed Carbonic Anhydrase (CA), Zn[CA] is used for the conversion of $CO_2$ to bicarbonate ($HCO_3^-$) [119].

Most of the enzymes being investigated in $CO_2$ reduction are naturally occurring and can denature easily under varying pH and temperature. Some key issues still remain that need to be considered when looking for further advancement in the biological catalysed $CO_2$ reduction. Firstly, the use of transition metals/metal ions incorporated unto enzymes protein ligands having high $CO_2$ binding affinity is vital for converting $CO_2$ molecules to desired products. Secondly, the depletion of NADH during catalytic $CO_2$ reduction reaction to $NAD^+$, as well as the higher stability of $CO_2$ molecule, resulting in its lower reactivity. To avoid this problem, it is necessary to regenerate NADH during $CO_2$ reduction. A separate NADH regeneration step which involve the use of combined chemical, photocatalytic, biocatalytic, and/or electrochemical reactions within a single set-up must be considered when engineering efficient bioinspired catalyst for $CO_2$ reduction.

**Funding**

This research received no external funding

**Acknowledgements**

Alli, Y.A. would like to express profound gratitude to LCC-CNRS and Dr K. Philippot for hosting in the engineering of metal nanoparticles group at LCC-CNRS-Toulouse, France, and providing him with laboratory space and enabling environment for postdoctoral research activities. Also, Ali, Y. A. appreciates Peculiar ultimate concerns limited for providing grant opportunity for postdoctoral research at CNRS-LCC. We would also appreciate NRF and Nelson Mandela University, South Africa for funding Funeka Matebese and Nokuthula Magida-Matomela.

**Conflicts of interest**

The authors declare no conflict of interest

**References**

[1] Y.A. Alli, P.O. Oladoye, A.T. Onawole, H. Anuar, S. Adewuyi, O.D. Ogunbiyi, K. Philippot, Photocatalysts for CO2 reduction and computational insights, Fuel. 344 (2023) 128101. https://doi.org/10.1016/J.FUEL.2023.128101.

[2] E.T. Sunquist, W.S. Broecker, The Carbon Cycle and Atmospheric CO 2 , Eos, Trans. Am. Geophys. Union. 67 (1986) 191. https://doi.org/10.1029/eo067i015p00191.

[3] UN Special Rapporteur, Safe Climate: A Report of the Special Rapporteur on Human Rights and the Environment, (2019) 44. https://wedocs.unep.org/bitstream/handle/20.500.11822/30158/Safe_Climate_Report.pdf?sequence=1&isAllowed=y.

[4] V. Kumaravel, J. Bartlett, S.C. Pillai, Photoelectrochemical Conversion of Carbon Dioxide (CO2) into Fuels and Value-Added Products, ACS Energy Lett. (2020) 486–519. https://doi.org/10.1021/acsenergylett.9b02585.

[5] H. Liu, S. Bansal, Metal halide perovskite nanostructures and quantum dots for photocatalytic CO2 reduction: prospects and challenges, Mater. Today Energy. 32 (2023). https://doi.org/10.1016/j.mtener.2022.101230.

[6] Y.A. Alli, P.O. Oladoye, O. Ejeromedoghene, O.M. Bankole, O.A. Alimi, E.O. Omotola, C.A. Olanrewaju, K. Philippot, A.S. Adeleye, A.S. Ogunlaja, Nanomaterials as catalysts for CO2 transformation into value-added products: A review, Sci. Total Environ. 868 (2023). https://doi.org/10.1016/j.scitotenv.2023.161547.

[7] Z. Moradi, S.Z. Jahromi, M. Ghaedi, Design of active photocatalysts and visible light photocatalysis, in: Interface Sci. Technol., Elsevier B.V., 2021: pp. 557–623. https://doi.org/10.1016/B978-0-12-818806-4.00012-7.

[8] L. Wang, C. Bie, J. Yu, Challenges of Z-scheme photocatalytic mechanisms, Trends Chem. 4 (2022) 973–983. https://doi.org/10.1016/j.trechm.2022.08.008.

[9] L. Zhang, J. Zhang, H. Yu, J. Yu, Emerging S-Scheme Photocatalyst, Adv. Mater. 34 (2022). https://doi.org/10.1002/adma.202107668.

[10] D.T. Nguyen, T.O. Do, Comprehensive Review for an Efficient Charge Transfer in Single Atomic Site Catalyst/Organic Polymers toward Photocatalytic CO2 Reduction, Adv. Mater. Interfaces. 10 (2023). https://doi.org/10.1002/admi.202201413.

[11] S. Liang, X. Zhong, Z. Zhong, B. Han, W. Chen, K. Song, H. Deng, Z. Lin, Biomimetic inspired porphyrin-based nanoframes for highly efficient photocatalytic CO2 reduction, Chem. Eng. J. 411 (2021) 128414. https://doi.org/10.1016/J.CEJ.2021.128414.

[12] H. Zhang, H. Liu, Z. Tian, D. Lu, Y. Yu, S. Cestellos-Blanco, K.K. Sakimoto, P. Yang, Bacteria photosensitized by intracellular gold nanoclusters for solar fuel production, Nat. Nanotechnol. 13 (2018) 900–905. https://doi.org/10.1038/s41565-018-0267-z.

[13] M.C.M. Yau, M. Hayes, S. Kalathil, Biocatalytic conversion of sunlight and carbon dioxide to solar fuels and chemicals, RSC Adv. 12 (2022) 16396–16411. https://doi.org/10.1039/d2ra00673a.

[14] C. J. Mallia, I. R. Baxendale, The Use of Gases in Flow Synthesis, Org. Process Res. & Dev. 20 (2015) 327–360. https://doi.org/10.1021/acs.oprd.5b00222.

[15] P. Zhai, Y. Li, M. Wang, J. Liu, Z. Cao, J. Zhang, Y. Xu, X. Liu, Y.W. Li, Q. Zhu, D. Xiao, X.D. Wen, D. Ma, Development of direct conversion of syngas to unsaturated

hydrocarbons based on Fischer-Tropsch route, Chem. 7 (2021) 3027–3051. https://doi.org/10.1016/J.CHEMPR.2021.08.019.

[16] T.W. Woolerton, S. Sheard, E. Pierce, S.W. Ragsdale, F.A. Armstrong, CO2 photoreduction at enzyme-modified metal oxide nanoparticles, Energy Environ. Sci. 4 (2011) 2393–2399. https://doi.org/10.1039/c0ee00780c.

[17] X. Ding, B. Yu, B. Han, H. Wang, T. Zheng, B. Chen, J. Wang, Z. Yu, T. Sun, X. Fu, D. Qi, J. Jiang, Porphyrin Coordination Polymer with Dual Photocatalytic Sites for Efficient Carbon Dioxide Reduction, ACS Appl. Mater. & Interfaces. 14 (2022) 8048–8057. https://doi.org/10.1021/acsami.1c23941.

[18] G. Zhao, H. Pang, G. Liu, P. Li, H. Liu, H. Zhang, L. Shi, J. Ye, Co-porphyrin/carbon nitride hybrids for improved photocatalytic CO2 reduction under visible light, Appl. Catal. B Environ. 200 (2017) 141–149. https://doi.org/10.1016/J.APCATB.2016.06.074.

[19] L. Lin, C. Hou, X. Zhang, Y. Wang, Y. Chen, T. He, Highly efficient visible-light driven photocatalytic reduction of CO2 over g-C3N4 nanosheets/tetra(4-carboxyphenyl)porphyrin iron(III) chloride heterogeneous catalysts, Appl. Catal. B Environ. 221 (2018) 312–319. https://doi.org/10.1016/J.APCATB.2017.09.033.

[20] H. Zhou, P. Li, J. Liu, Z. Chen, L. Liu, D. Dontsova, R. Yan, T. Fan, D. Zhang, J. Ye, Biomimetic polymeric semiconductor based hybrid nanosystems for artificial photosynthesis towards solar fuels generation via CO2 reduction, Nano Energy. 25 (2016) 128–135. https://doi.org/10.1016/j.nanoen.2016.04.049.

[21] J. Shipp, S. Parker, S. Spall, S.L. Peralta-Arriaga, C.C. Robertson, D. Chekulaev, P. Portius, S. Turega, A. Buckley, R. Rothman, J.A. Weinstein, Photocatalytic Reduction of CO2to CO in Aqueous Solution under Red-Light Irradiation by a Zn-Porphyrin-Sensitized Mn(I) Catalyst, Inorg. Chem. 61 (2022) 13281–13292. https://doi.org/10.1021/acs.inorgchem.2c00091.

[22] Y.S. Chaudhary, T.W. Woolerton, C.S. Allen, J.H. Warner, E. Pierce, S.W. Ragsdale, F.A. Armstrong, Visible light-driven CO2 reduction by enzyme coupled CdS nanocrystals, Chem. Commun. 48 (2012) 58–60. https://doi.org/10.1039/c1cc16107e.

[23] S. Lee, S. Kim, C. Park, G.H. Moon, H.J. Son, J.O. Baeg, W. Kim, W. Choi, Nafion-Assisted Noncovalent Assembly of Molecular Sensitizers and Catalysts for Sustained Photoreduction of CO2 to CO, ACS Sustain. Chem. Eng. 8 (2020) 3709–3717. https://doi.org/10.1021/acssuschemeng.9b06797.

[24] G.K.S.P. G. A. Olah, A. Goeppert, Beyond Oil and Gas: The Methanol Economy, 2nd ed, Wiley-VCH, Weinheim, Germany, 2009. https://doi.org/10.1002/9783527627806.

[25] F. Dalena, A. Senatore, A. Marino, A. Gordano, M. Basile, A. Basile, Methanol Production and Applications: An Overview, Elsevier B.V., 2018. https://doi.org/10.1016/B978-0-444-63903-5.00001-7.

[26] G. Bozzano, F. Manenti, Efficient methanol synthesis: Perspectives, technologies and optimization strategies, Prog. Energy Combust. Sci. 56 (2016) 71–105. https://doi.org/10.1016/j.pecs.2016.06.001.

[27] A. Abbas, K. Qadeer, A. Al-Hinai, M.H. Tarar, M.A. Qyyum, A.H. Al-Muhtaseb, R. Al Abri, M. Lee, R. Dickson, Process development and policy implications for large scale deployment of solar-driven electrolysis-based renewable methanol production, Green Chem. (2022) 7630–7643. https://doi.org/10.1039/d2gc01993k.

[28] A. González-Garay, M.S. Frei, A. Al-Qahtani, C. Mondelli, G. Guillén-Gosálbez, J. Pérez-Ramírez, Plant-to-planet analysis of CO2-based methanol processes, Energy Environ. Sci. 12 (2019) 3425–3436. https://doi.org/10.1039/c9ee01673b.

[29] P. Sharma, S. Kumar, O. Tomanec, M. Petr, J. Zhu Chen, J.T. Miller, R.S. Varma, M.B. Gawande, R. Zbořil, Carbon Nitride-Based Ruthenium Single Atom Photocatalyst for CO2 Reduction to Methanol, Small. 17 (2021). https://doi.org/10.1002/smll.202006478.

[30] S.M. Aliwi, K.F. Al-Jubori, Photoreduction of CO2 by metal sulphide semiconductors in presence of H2S, Sol. Energy Mater. 18 (1989) 223–229. https://doi.org/10.1016/0165-1633(89)90056-7.

[31] Y. Yang, Y.X. Pan, X. Tu, C. jun Liu, Nitrogen doping of indium oxide for enhanced photocatalytic reduction of CO2 to methanol, Nano Energy. 101 (2022) 107613.

https://doi.org/10.1016/J.NANOEN.2022.107613.

[32] K. Kočí, K. Matějů, L. Obalová, S. Krejčíková, Z. Lacný, D. Plachá, L. Čapek, A. Hospodková, O. Šolcová, Effect of silver doping on the TiO2 for photocatalytic reduction of CO2, Appl. Catal. B Environ. 96 (2010) 239–244. https://doi.org/10.1016/J.APCATB.2010.02.030.

[33] R.K. Yadav, J.O. Lee, A. Kumar, N.J. Park, D. Yadav, J.Y. Kim, J.O. Baeg, Highly Improved Solar Energy Harvesting for Fuel Production from CO2 by a Newly Designed Graphene Film Photocatalyst, Sci. Rep. 8 (2018) 1–10. https://doi.org/10.1038/s41598-018-35135-7.

[34] D. Yadav, R.K. Yadav, A. Kumar, N.J. Park, J.Y. Kim, J.O. Baeg, Fullerene polymer film as a highly efficient photocatalyst for selective solar fuel production from CO2, J. Appl. Polym. Sci. 137 (2020) 1–9. https://doi.org/10.1002/app.48536.

[35] B. Aurian-Blajeni, M. Halmann, J. Manassen, Photoreduction of carbon dioxide and water into formaldehyde and methanol on semiconductor materials, Sol. Energy. 25 (1980) 165–170. https://doi.org/10.1016/0038-092X(80)90472-7.

[36] Y. Amao, R. Kataoka, Methanol production from CO2 with the hybrid system of biocatalyst and organo-photocatalyst, Catal. Today. 307 (2018) 243–247. https://doi.org/10.1016/j.cattod.2017.12.029.

[37] H.C. Hsu, I. Shown, H.Y. Wei, Y.C. Chang, H.Y. Du, Y.G. Lin, C.A. Tseng, C.H. Wang, L.C. Chen, Y.C. Lin, K.H. Chen, Graphene oxide as a promising photocatalyst for CO 2 to methanol conversion, Nanoscale. 5 (2012) 262–268. https://doi.org/10.1039/C2NR31718D.

[38] K. Kočí, L. Obalová, Z. Lacný, Photocatalytic reduction of CO2 over TiO2 based catalysts, Chem. Pap. 62 (2008) 1–9. https://doi.org/10.2478/S11696-007-0072-X/MACHINEREADABLECITATION/RIS.

[39] S. Chakrabarti, B. Chaudhuri, S. Bhattacharjee, A.K. Ray, B.K. Dutta, Photo-reduction of hexavalent chromium in aqueous solution in the presence of zinc oxide as semiconductor

catalyst, Chem. Eng. J. 153 (2009) 86–93. https://doi.org/10.1016/J.CEJ.2009.06.021.

[40] M.S. Ramyashree, S. Shanmuga Priya, N.C. Freudenberg, K. Sudhakar, M. Tahir, Metal-organic framework-based photocatalysts for carbon dioxide reduction to methanol: A review on progress and application, J. CO2 Util. 43 (2021) 101374. https://doi.org/10.1016/J.JCOU.2020.101374.

[41] S.M. Albukhari, A.A. Ismail, Highly Dispersed Pt Nanoparticle-Doped Mesoporous ZnO Photocatalysts for Promoting Photoconversion of CO2to Methanol, ACS Omega. 06 (2021) 43. https://doi.org/10.1021/acsomega.1c03259.

[42] S.P. Cheng, L.W. Wei, H.P. Wang, Photocatalytic reduction of CO2 to methanol by Cu2 O/TiO2 heterojunctions, Sustain. 14 (2022). https://doi.org/10.3390/SU14010374.

[43] O. Quiroz-Cardoso, V. Suárez, S. Oros-Ruiz, M. Quintana, S. Ramírez-Rave, M. Suárez-Quezada, R. Gómez, Synthesis of Ni/GO-TiO2 composites for the photocatalytic hydrogen production and CO2 reduction to methanol, Top. Catal. 65 (2022) 1015–1027. https://doi.org/10.1007/s11244-022-01643-0.

[44] I.H. Tseng, Y.M. Sung, P.Y. Chang, C.Y. Chen, Anatase TiO 2 -decorated graphitic carbon nitride for photocatalytic conversion of carbon dioxide, Polymers (Basel). 11 (2019) 1–16. https://doi.org/10.3390/polym11010146.

[45] I. Tseng, Z. Liu, P. Chang, Bio-friendly titania-grafted chitosan fi lm with biomimetic surface structure for photocatalytic application, Carbohydr. Polym. 230 (2020) 115584. https://doi.org/10.1016/j.carbpol.2019.115584.

[46] Y.N. Kavil, Y.A. Shaban, R.K. Al Farawati, M.I. Orif, M. Zobidi, S.U.M. Khan, Photocatalytic conversion of CO2 into methanol over Cu-C/TiO2 nanoparticles under UV light and natural sunlight, J. Photochem. Photobiol. A Chem. 347 (2017) 244–253. https://doi.org/10.1016/j.jphotochem.2017.07.046.

[47] S. Schlager, A. Dibenedetto, M. Aresta, D.H. Apaydin, L.M. Dumitru, H. Neugebauer, N.S. Sariciftci, Biocatalytic and Bioelectrocatalytic Approaches for the Reduction of Carbon Dioxide using Enzymes, Energy Technol. 5 (2017) 812–821.

https://doi.org/10.1002/ente.201600610.

[48] M. Zezzi Do Valle Gomes, G. Masdeu, P. Eiring, A. Kuhlemann, M. Sauer, B. Åkerman, A.E.C. Palmqvist, Improved biocatalytic cascade conversion of CO2to methanol by enzymes Co-immobilized in tailored siliceous mesostructured cellular foams, Catal. Sci. Technol. 11 (2021) 6952–6959. https://doi.org/10.1039/d1cy01354h.

[49] Z. Zhang, J. Tong, X. Meng, Y. Cai, S. Ma, F. Huo, J. Luo, B.H. Xu, S. Zhang, M. Pinelo, Development of an Ionic Porphyrin-Based Platform as a Biomimetic Light-Harvesting Agent for High-Performance Photoenzymatic Synthesis of Methanol from CO2, ACS Sustain. Chem. Eng. 9 (2021) 11503–11511. https://doi.org/10.1021/ACSSUSCHEMENG.1C03737/SUPPL_FILE/SC1C03737_SI_001.PDF.

[50] S. Chaubey, P. Singh, C. Singh, S. Singh, S. Shreya, R.K. Yadav, S. Mishra, Y. jin Jeong, B.K. Biswas, T.W. Kim, Ultra-efficient synthesis of bamboo-shape porphyrin framework for photocatalytic CO2 reduction and consecutive C-S/C-N bonds formation, J. CO2 Util. 59 (2022) 101968. https://doi.org/10.1016/j.jcou.2022.101968.

[51] Y. Tian, Y. Zhou, Y. Zong, J. Li, N. Yang, M. Zhang, Z. Guo, H. Song, Construction of Functionally Compartmental Inorganic Photocatalyst-Enzyme System via Imitating Chloroplast for Efficient Photoreduction of CO2 to Formic Acid, ACS Appl. Mater. Interfaces. 12 (2020) 34795–34805. https://doi.org/10.1021/acsami.0c06684.

[52] R.K. Yadav, G.H. Oh, N.J. Park, A. Kumar, K.J. Kong, J.O. Baeg, Highly selective solar-driven methanol from CO2 by a photocatalyst/biocatalyst integrated system, J. Am. Chem. Soc. 136 (2014) 16728–16731. https://doi.org/10.1021/ja509650r.

[53] X. Ji, Z. Su, P. Wang, G. Ma, S. Zhang, Integration of Artificial Photosynthesis System for Enhanced Electronic Energy-Transfer Efficacy: A Case Study for Solar-Energy Driven Bioconversion of Carbon Dioxide to Methanol, Small. 12 (2016) 4753–4762. https://doi.org/10.1002/smll.201600707.

[54] G. Yisilamu, H. Maimaiti, A. Awati, D. Zhang, F. Sun, B. Xu, Preparation of Cuprous Oxide Nanoparticles Coated with Aminated Cellulose for the Photocatalytic Reduction of

Carbon Dioxide to Methanol, Energy Technol. 6 (2018) 1168–1177. https://doi.org/10.1002/ENTE.201700689.

[55] M. Belay Getahun, E. Budi Santiko, T. Imae, C.L. Chiang, Y.G. Lin, Photocatalytic conversion of gaseous carbon dioxide to methanol on CuO/ZnO-embedded carbohydrate polymer films, Appl. Surf. Sci. 604 (2022) 154515. https://doi.org/10.1016/j.apsusc.2022.154515.

[56] S. Rouf, Y.E. Greish, S. Al-Zuhair, Immobilization of formate dehydrogenase in metal organic frameworks for enhanced conversion of carbon dioxide to formate, Chemosphere. 267 (2021) 128921. https://doi.org/10.1016/j.chemosphere.2020.128921.

[57] H.Y. K. Tamaki, P. Verma, T. Yoshii, T. Shimojitosho, Y. Kuwahara, K. Mori, Design of Au nanorods-based plasmonic catalyst in combination with nanohybrid Pd-rGO layer for boosting CO2 hydrogenation to formic acid under visible light irradiation, Catal. Today. (2022). https://doi.org/10.1016/j.cattod.2022.06.010.

[58] T. Brütsch, G. Jaffuel, A. Vallat, T.C.J. Turlings, M. Chapuisat, Wood ants produce a potent antimicrobial agent by applying formic acid on tree-collected resin, Ecol. Evol. 7 (2017) 2249–2254. https://doi.org/10.1002/ece3.2834.

[59] B. Feng, Z. Zhang, J. Wang, D. Yang, Q. Li, Y. Liu, H. Gai, T. Huang, H. Song, Synthesis of hydrophobic Pd-poly(ionic liquid)s with excellent CO2 affinity to efficiently catalyze CO2 hydrogenation to formic acid, Fuel. 325 (2022) 124853. https://doi.org/10.1016/j.fuel.2022.124853.

[60] X. Hu, M. Luo, M. ur Rehman, J. Sun, H.A.S.M. Yaseen, F. Irshad, Y. Zhao, S. Wang, X. Ma, Mechanistic insight into the electron-donation effect of modified ZIF-8 on Ru for CO2 hydrogenation to formic acid, J. CO2 Util. 60 (2022) 101992. https://doi.org/10.1016/j.jcou.2022.101992.

[61] P. Duarah, D. Haldar, V.S.K. Yadav, M.K. Purkait, Progress in the electrochemical reduction of CO2 to formic acid: A review on current trends and future prospects, J. Environ. Chem. Eng. 9 (2021) 106394. https://doi.org/10.1016/j.jece.2021.106394.

[62] H.W. Langmi, N. Engelbrecht, P.M. Modisha, D. Bessarabov, Hydrogen storage, Elsevier B.V., 2002.

[63] J.D. Medrano-García, R. Ruiz-Femenia, J.A. Caballero, Multi-objective Optimization of a Carbon Dioxide Utilization Superstructure for the Synthesis of Formic and Acetic Acid, Comput. Aided Chem. Eng. 43 (2018) 1419–1424. https://doi.org/10.1016/B978-0-444-64235-6.50248-5.

[64] N. Yan, K. Philippot, Transformation of CO2 by using nanoscale metal catalysts: cases studies on the formation of formic acid and dimethylether, Curr. Opin. Chem. Eng. 20 (2018) 86–92. https://doi.org/10.1016/j.coche.2018.03.006.

[65] S.C. Huang, C.C. Cheng, Y.H. Lai, C.Y. Lin, Sustainable and selective formic acid production from photoelectrochemical methanol reforming at near-neutral pH using nanoporous nickel-iron oxyhydroxide-borate as the electrocatalyst, Chem. Eng. J. 395 (2020) 125176. https://doi.org/10.1016/j.cej.2020.125176.

[66] Y.A. Alli, S. Adewuyi, B.S. Bada, S. Thomas, H. Anuar, Quaternary Trimethyl Chitosan Chloride Capped Bismuth Nanoparticles with Positive Surface Charges: Catalytic and Antibacterial Activities, J. Clust. Sci. 33 (2022) 2311–2324. https://doi.org/10.1007/s10876-021-02156-8.

[67] Y.A. Alli, O. Ejeromedoghene, A. Oladipo, S. Adewuyi, S.A. Amolegbe, H. Anuar, S. Thomas, Compressed Hydrogen-Induced Synthesis of Quaternary Trimethyl Chitosan-Silver Nanoparticles with Dual Antibacterial and Antifungal Activities, ACS Appl. Bio Mater. 5 (2022) 5240–5254. https://doi.org/10.1021/acsabm.2c00670.

[68] D. Wu, W. Chen, X. Wang, X.Z. Fu, J.L. Luo, Metal-support interaction enhanced electrochemical reduction of CO2 to formate between graphene and Bi nanoparticles, J. CO2 Util. 37 (2020) 353–359. https://doi.org/10.1016/j.jcou.2020.02.007.

[69] M. Andérez-Fernández, E. Pérez, S. Ferrero, C.M. Álvarez, J. Gumiel, Á. Martín, M.D. Bermejo, Simultaneous formic acid production by hydrothermal CO2 reduction and biomass derivatives conversion in a continuous reactor, Chem. Eng. J. 453 (2023) 139741. https://doi.org/10.1016/j.cej.2022.139741.

[70] F.J. Gu, Y.Z. Wang, Z.H. Meng, W.F. Liu, L.Y. Qiu, A coupled photocatalytic/enzymatic system for sustainable conversion of CO2 to formate, Catal. Commun. 136 (2020) 105903. https://doi.org/10.1016/j.catcom.2019.105903.

[71] Y.F. Tian, D. Li, J. Wu, J. Liu, C. Li, G. Liu, D. Chen, Electroreduction of CO2 to formate with excellent selectivity and stability on nano-dendrite Bi film electrode, J. CO2 Util. 43 (2021) 101360. https://doi.org/10.1016/j.jcou.2020.101360.

[72] X. Zhang, T. Lei, Y. Liu, J. Qiao, Enhancing CO2 electrolysis to formate on facilely synthesized Bi catalysts at low overpotential, Appl. Catal. B Environ. 218 (2017) 46–50. https://doi.org/10.1016/j.apcatb.2017.06.032.

[73] A. Rosas-Hernández, H. Junge, M. Beller, Photochemical Reduction of Carbon Dioxide to Formic Acid using Ruthenium(II)-Based Catalysts and Visible Light, ChemCatChem. 7 (2015) 3316–3321. https://doi.org/10.1002/cctc.201500494.

[74] R. Cauwenbergh, S. Das, Photochemical reduction of carbon dioxide to formic acid, Green Chem. 23 (2021) 2553–2574. https://doi.org/10.1039/d0gc04040a.

[75] H. T. Gao, X. Wen, T. Xie, N. Han, K. Sun, L. Han, S. Wang, Y. Zhang, Y. Kuang, X, Morphology effects of bismuth catalysts on electroreduction of carbon dioxide into formate, Electrochim. Acta. 305 (2019) 388–393. https://doi.org/10.1016/j.electacta.2019.03.066.

[76] A.T. Cannon, C.T. Saouma, Ru catalyzed hydrogenation of CO2 to formate under basic and acidic conditions, Polyhedron. 207 (2021) 115375. https://doi.org/10.1016/j.poly.2021.115375.

[77] G. Pietricola, C. Ottone, D. Fino, T. Tommasi, Enzymatic reduction of CO2 to formic acid using FDH immobilized on natural zeolite, J. CO2 Util. 42 (2020) 101343. https://doi.org/10.1016/j.jcou.2020.101343.

[78] Z. Zhang, T. Vasiliu, F. Li, A. Laaksonen, F. Mocci, X. Ji, Electrochemically driven efficient enzymatic conversion of CO2 to formic acid with artificial cofactors, J. CO2 Util. 52 (2021) 101679. https://doi.org/10.1016/j.jcou.2021.101679.

[79] C.D. Tang, Z.H. Zhang, H.L. Shi, Y.L. Xie, T.T. Yang, Y.F. Lu, S.P. Zhang, F.H. Bai, Y.C. Kan, L.G. Yao, Directed evolution of formate dehydrogenase and its application in the biosynthesis of L-phenylglycine from phenylglyoxylic acid, Mol. Catal. 513 (2021) 111666. https://doi.org/10.1016/J.MCAT.2021.111666.

[80] S. Hakopian, D. Niks, R. Hille, The air-inactivation of formate dehydrogenase FdsDABG from Cupriavidus necator, J. Inorg. Biochem. 231 (2022) 111788. https://doi.org/10.1016/J.JINORGBIO.2022.111788.

[81] N. Hernández-Ibáñez, A. Gomis-Berenguer, V. Montiel, C.O. Ania, J. Iniesta, Fabrication of a biocathode for formic acid production upon the immobilization of formate dehydrogenase from Candida boidinii on a nanoporous carbon, Chemosphere. 291 (2022) 133117. https://doi.org/10.1016/j.chemosphere.2021.133117.

[82] S. Yu, P. Lv, P. Xue, K. Wang, Q. Yang, J. Zhou, M. Wang, L. Wang, B. Chen, T. Tan, Light-driven enzymatic nanosystem for highly selective production of formic acid from CO2, Chem. Eng. J. 420 (2021) 127649. https://doi.org/10.1016/j.cej.2020.127649.

[83] Y. Wang, M. Li, Z. Zhao, W. Liu, Effect of carbonic anhydrase on enzymatic conversion of CO2 to formic acid and optimization of reaction conditions, J. Mol. Catal. B Enzym. 116 (2015) 89–94. https://doi.org/10.1016/j.molcatb.2015.03.014.

[84] S. Zhang, J. Shi, Y. Sun, Y. Wu, Y. Zhang, Z. Cai, Y. Chen, C. You, P. Han, Z. Jiang, Artificial Thylakoid for the Coordinated Photoenzymatic Reduction of Carbon Dioxide, ACS Catal. 9 (2019) 3913–3925. https://doi.org/10.1021/acscatal.9b00255.

[85] P. Zhang, J. Hu, Y. Shen, X. Yang, J. Qu, F. Du, W. Sun, C.M. Li, Photoenzymatic Catalytic Cascade System of a Pyromellitic Diimide/g-C3N4 Heterojunction to Efficiently Regenerate NADH for Highly Selective CO2 Reduction toward Formic Acid, ACS Appl. Mater. Interfaces. 13 (2021) 46650–46658. https://doi.org/10.1021/acsami.1c13167.

[86] R.K. Yadav, A. Kumar, N.J. Park, D. Yadav, J.O. Baeg, New Carbon Nanodots-Silica Hybrid Photocatalyst for Highly Selective Solar Fuel Production from CO2, ChemCatChem. 9 (2017) 3153–3159. https://doi.org/10.1002/cctc.201700789.

[87] S. Kumar, R.K. Yadav, K. Ram, A. Aguiar, J. Koh, A.J.F.N. Sobral, Graphene oxide modified cobalt metallated porphyrin photocatalyst for conversion of formic acid from carbon dioxide, J. CO2 Util. 27 (2018) 107–114. https://doi.org/10.1016/j.jcou.2018.07.008.

[88] B. Fall, C. Gaye, M. Niang, Y.A. Alli, A.K.D. Diaw, M. Fall, S. Thomas, H. Randriamahazaka, Removal of Toxic Chromium Ions in Aqueous Medium Using a New Sorbent Based on rGO@CNT@Fe2O3, Chem. Africa. 5 (2022) 1809–1821. https://doi.org/10.1007/s42250-022-00499-x.

[89] X. Ji, J. Wang, L. Mei, W. Tao, A. Barrett, Z. Su, S. Wang, G. Ma, J. Shi, S. Zhang, Porphyrin/SiO2/Cp*Rh(bpy)Cl Hybrid Nanoparticles Mimicking Chloroplast with Enhanced Electronic Energy Transfer for Biocatalyzed Artificial Photosynthesis, Adv. Funct. Mater. 28 (2018) 1–14. https://doi.org/10.1002/adfm.201705083.

[90] X. Ji, Y. Kang, T. Fan, Q. Xiong, S. Zhang, W. Tao, H. Zhang, An antimonene/Cp∗Rh(phen)Cl/black phosphorus hybrid nanosheet-based Z-scheme artificial photosynthesis for enhanced photo/bio-catalytic CO2 reduction, J. Mater. Chem. A. 8 (2020) 323–333. https://doi.org/10.1039/c9ta11167k.

[91] S. Singh, R.K. Yadav, T.W. Kim, C. Singh, P. Singh, A. P. Singh, A.K. Singh, A.K. Singh, J.O. Baeg, S.K. Gupta, Design of a graphitic carbon nitride catalytic-biocatalytic system for solar light-based CO2 production, React. Chem. Eng. 7 (2022) 1566–1572. https://doi.org/10.1039/d2re00079b.

[92] Y. Zhang, J. Liu, Bioinspired Photocatalytic NADH Regeneration by Covalently Metalated Carbon Nitride for Enhanced CO2 Reduction, Chem. - A Eur. J. 28 (2022) e202201430. https://doi.org/10.1002/chem.202201430.

[93] Y. Cheng, J. Shi, Y. Wu, X. Wang, Y. Sun, Z. Cai, Y. Chen, Z. Jiang, Intensifying Electron Utilization by Surface-Anchored Rh Complex for Enhanced Nicotinamide Cofactor Regeneration and Photoenzymatic CO2 Reduction, Research. 2021 (2021) 1–11. https://doi.org/10.34133/2021/8175709.

[94] A. Kumar, R.K. Yadav, N.J. Park, J.O. Baeg, Facile One-Pot Two-Step Synthesis of

Novel in Situ Selenium-Doped Carbon Nitride Nanosheet Photocatalysts for Highly Enhanced Solar Fuel Production from CO2, ACS Appl. Nano Mater. 1 (2018) 47–54. https://doi.org/10.1021/acsanm.7b00024.

[95] S. Kumar, R.K. Yadav, S. Gupta, S. Yeon Choi, T. Wu Kim, A Spherical Photocatalyst To Emulate Natural Photosynthesis For The Production of Formic Acid From CO2, J. Photochem. Photobiol. A Chem. (2023) 114545. https://doi.org/10.1016/J.JPHOTOCHEM.2023.114545.

[96] N. Singh, D. Yadav, S. V. Mulay, J.Y. Kim, N.J. Park, J.O. Baeg, Band Gap Engineering in Solvochromic 2D Covalent Organic Framework Photocatalysts for Visible Light-Driven Enhanced Solar Fuel Production from Carbon Dioxide, ACS Appl. Mater. Interfaces. 13 (2021) 14122–14131. https://doi.org/10.1021/acsami.0c21117.

[97] Y. Chen, P. Li, J. Zhou, C.T. Buru, L. Aorević, P. Li, X. Zhang, M.M. Cetin, J.F. Stoddart, S.I. Stupp, M.R. Wasielewski, O.K. Farha, Integration of Enzymes and Photosensitizers in a Hierarchical Mesoporous Metal-Organic Framework for Light-Driven CO2 Reduction, J. Am. Chem. Soc. 142 (2020) 1768–1773. https://doi.org/10.1021/jacs.9b12828.

[98] J.A. Kim, S. Kim, J. Lee, J.O. Baeg, J. Kim, Photochemical production of NADH using cobaloxime catalysts and visible-light energy, Inorg. Chem. 51 (2012) 8057–8063. https://doi.org/10.1021/ic300185n.

[99] T. Welton, Solvents and sustainable chemistry, Proc. R. Soc. A Math. Phys. Eng. Sci. 471 (2015). https://doi.org/10.1098/rspa.2015.0502.

[100] G. Deshmukh, H. Manyar, Production Pathways of Acetic Acid and Its Versatile Applications in the Food Industry, in: Biotechnol. Appl. Biomass, IntechOpen, 2021. https://doi.org/10.5772/intechopen.92289.

[101] P. Gai, W. Yu, H. Zhao, R. Qi, F. Li, L. Liu, F. Lv, S. Wang, Solar-Powered Organic Semiconductor–Bacteria Biohybrids for CO2 Reduction into Acetic Acid, Angew. Chemie - Int. Ed. 59 (2020) 7224–7229. https://doi.org/10.1002/anie.202001047.

[102] A. Tharak, R. Katakojwala, S. Kajla, S. Venkata Mohan, Chemolithoautotrophic reduction of CO2 to Acetic acid in Gas and Gas-electro fermentation systems: Enrichment, Microbial dynamics, and Sustainability assessment, Chem. Eng. J. (2022) 140200. https://doi.org/10.1016/j.cej.2022.140200.

[103] H. Wang, Y. Zhao, Z. Ke, B. Yu, R. Li, Y. Wu, Z. Wang, J. Han, Z. Liu, Synthesis of renewable acetic acid from CO2 and lignin over an ionic liquid-based catalytic system, Chem. Commun. 55 (2019) 3069–3072. https://doi.org/10.1039/c9cc00819e.

[104] K.K. Sakimoto, A.B. Wong, P. Yang, Self-photosensitization of nonphotosynthetic bacteria for solar-to-chemical production, Science (80-. ). 351 (2016) 74–77. https://doi.org/10.1126/science.aad3317.

[105] B. Mondal, J. Song, F. Neese, S. Ye, Bio-inspired mechanistic insights into CO2 reduction, Curr. Opin. Chem. Biol. 25 (2015) 103–109. https://doi.org/10.1016/J.CBPA.2014.12.022.

[106] S.N. Habisreutinger, L. Schmidt-Mende, J.K. Stolarczyk, Photocatalytic reduction of CO2 on TiO2 and other semiconductors, Angew. Chem. Int. Ed. Engl. 52 (2013) 7372–7408. https://doi.org/10.1002/ANIE.201207199.

[107] R. Gusain, P. Kumar, O.P. Sharma, S.L. Jain, O.P. Khatri, Reduced graphene oxide–CuO nanocomposites for photocatalytic conversion of CO2 into methanol under visible light irradiation, Appl. Catal. B Environ. 181 (2016) 352–362. https://doi.org/10.1016/J.APCATB.2015.08.012.

[108] Q. Zhai, S. Xie, W. Fan, Q. Zhang, Y. Wang, W. Deng, Y. Wang, Photocatalytic Conversion of Carbon Dioxide with Water into Methane: Platinum and Copper(I) Oxide Co-catalysts with a Core–Shell Structure, Angew. Chemie Int. Ed. 52 (2013) 5776–5779. https://doi.org/10.1002/ANIE.201301473.

[109] G. Mele, C. Annese, A. De Riccardis, C. Fusco, L. Palmisano, G. Vasapollo, L. D'Accolti, Turning lipophilic phthalocyanines/TiO2 composites into efficient photocatalysts for the conversion of CO2 into formic acid under UV–vis light irradiation, Appl. Catal. A Gen. 481 (2014) 169–172. https://doi.org/10.1016/J.APCATA.2014.05.008.

[110] Y.A. Wu, I. McNulty, C. Liu, K.C. Lau, Q. Liu, A.P. Paulikas, C.J. Sun, Z. Cai, J.R. Guest, Y. Ren, V. Stamenkovic, L.A. Curtiss, Y. Liu, T. Rajh, Facet-dependent active sites of a single Cu2O particle photocatalyst for CO2 reduction to methanol, Nat. Energy 2019 411. 4 (2019) 957–968. https://doi.org/10.1038/s41560-019-0490-3.

[111] S.-M. Park, A. Razzaq, Y.H. Park, S. Sorcar, Y. Park, C.A. Grimes, S.-I. In, Hybrid CuxO−TiO2 Heterostructured Composites for Photocatalytic CO2 Reduction into Methane Using Solar Irradiation: Sunlight into Fuel, (2016). https://doi.org/10.1021/acsomega.6b00164.

[112] Z. Otgonbayar, K. Youn Cho, W.-C. Oh, Novel Micro and Nanostructure of a AgCuInS2−Graphene−TiO2 Ternary Composite for Photocatalytic CO2 Reduction for Methanol Fuel, Cite This ACS Omega. 5 (2020). https://doi.org/10.1021/acsomega.0c02498.

[113] M. Can, F.A. Armstrong, S.W. Ragsdale, Structure, Function, and Mechanism of the Nickel Metalloenzymes, CO Dehydrogenase, and Acetyl-CoA Synthase, (2014). https://doi.org/10.1021/cr400461p.

[114] E. V. Filippova, K.M. Polyakov, T. V. Tikhonova, T.N. Stekhanova, K.M. Boĭko, V.O. Popov, Structure of a new crystal modification of the bacterial NAD-dependent formate dehydrogenase with a resolution of 2.1 Å, Crystallogr. Reports. 50 (2005) 796–800. https://doi.org/10.1134/1.2049398.

[115] I.G. Shabalin, K.M. Polyakov, V.I. Tishkov, V.O. Popov, Atomic Resolution Crystal Structure of NAD +Dependent Formate Dehydrogenase from Bacterium Moraxella sp. C-1, Acta Naturae. 1 (2009) 89–93. https://doi.org/10.32607/20758251-2009-1-3-89-93.

[116] J.S. Blanchard, W.W. Cleland, Kinetic and Chemical Mechanisms of Yeast Formate Dehydrogenase, Biochemistry. 19 (1980) 3543–3550. https://doi.org/10.1021/BI00556A020/ASSET/BI00556A020.FP.PNG_V03.

[117] N.S. Rotberg, W.W. Cleland, Secondary 15N isotope effects on the reactions catalyzed by alcohol and formate dehydrogenases, Biochemistry. 30 (1991) 4068–4071. https://doi.org/10.1021/BI00230A035.

[118] V.S. Lamzin, Z. Dauter, V.O. Popov, E.H. Harutyunyan, K.S. Wilson, High resolution structures of holo and apo formate dehydrogenase, J. Mol. Biol. 236 (1994) 759–785. https://doi.org/10.1006/JMBI.1994.1188.

[119] R. Castillo, M. Oliva, S. Martí, V. Moliner, A theoretical study of the catalytic mechanism of formate dehydrogenase, J. Phys. Chem. B. 112 (2008) 10013–10022. https://doi.org/10.1021/JP8025896/SUPPL_FILE/JP8025896-FILE001.PDF.

[120] Z. Zhao, P. Yu, B.K. Shanbhag, P. Holt, Y.L. Zhong, L. He, Sustainable Recycling of Formic Acid by Bio-Catalytic CO2 Capture and Re-Hydrogenation, C. 5 (2019) 22. https://doi.org/10.3390/C5020022.

[121] T. Reda, C.M. Plugge, N.J. Abram, J. Hirst, Reversible interconversion of carbon dioxide and formate by an electroactive enzyme, Proc. Natl. Acad. Sci. U. S. A. 105 (2008) 10654–10658. https://doi.org/10.1073/PNAS.0801290105.

[122] S. Srikanth, Y. Alvarez-Gallego, K. Vanbroekhoven, D. Pant, Enzymatic Electrosynthesis of Formic Acid through Carbon Dioxide Reduction in a Bioelectrochemical System: Effect of Immobilization and Carbonic Anhydrase Addition, ChemPhysChem. 18 (2017) 3174–3181. https://doi.org/10.1002/CPHC.201700017.